

1 **Organic aerosol source apportionment by offline-AMS over a full** 2 **year in Marseille**

3

4 **Carlo Bozzetti¹, Imad El Haddad¹, Dalia Salameh^{2,7}, Kaspar Rudolf Daellenbach¹, Paola**
5 **Fermo³, Raquel Gonzalez³, Maria Cruz Minguillón⁴, Yoshiteru Iinuma⁵, Laurent**
6 **Poulain⁵, Emanuel Müller⁶, Jay Gates Slowik¹, Jean-Luc Jaffrezo⁷, Urs Baltensperger¹,**
7 **Nicolas Marchand², and André Stephan Henry Prévôt¹**

8 [1]{Paul Scherrer Institute (PSI), 5232 Villigen-PSI, Switzerland }

9 [2]{Aix Marseille Univ., CNRS, LCE, 13331 Marseille, France }

10 [3]{Università degli Studi di Milano, 20133 Milano, Italy }

11 [4]{Institute of Environmental Assessment and Water Research (IDAEA), CSIC, 08034
12 Barcelona, Spain }

13 [5]{Leibniz Institute für Troposphärenforschung, 04318 Leipzig, Germany }

14 [6]{Eawag, 8600 Dübendorf, Switzerland }

15 [7]{Université Grenoble Alpes, CNRS, LGGE, 38000 Grenoble, France }

16

17 Correspondence to: A. S. H. Prévôt (andre.prevot@psi.ch)

18 N. Marchand (nicolas.marchand@univ-amu.fr)

19

20 **Abstract**

21 We investigated the seasonal trends of OA sources affecting the air quality of Marseille
22 (France) which is the largest harbor of the Mediterranean Sea. This was achieved by
23 measurements of nebulized filter extracts using an aerosol mass spectrometer (offline-AMS).
24 In total 216 PM_{2.5} (particulate matter with an aerodynamic diameter <2.5 μm) filter samples
25 were collected over 1 year from August 2011 to July 2012. These filters were used to create
26 54 composite samples which were analyzed by offline-AMS. The same samples were also
27 analyzed for major water-soluble ions, metals, elemental and organic carbon (EC/OC), and
28 organic markers, including n-alkanes, hopanes, polyaromatic hydrocarbons (PAHs), lignin

1 and cellulose pyrolysis products and nitrocatechols. The application of positive matrix
2 factorization (PMF) to the water-soluble AMS spectra enabled the extraction of five factors,
3 related to hydrocarbon-like OA (HOA), cooking OA (COA), biomass burning OA (BBOA),
4 oxygenated OA (OOA), and an industry-related OA (INDOA). Seasonal trends and relative
5 contributions of OA sources were compared with the source apportionment of OA spectra
6 collected from the AMS field deployment at the same station but in different years and for
7 shorter monitoring periods (February 2011 and July 2008). Online- and offline-AMS source
8 apportionment revealed comparable seasonal contribution of the different OA sources.
9 Results revealed that BBOA was the dominant source during winter representing on average
10 48% of the OA, while during summer the main OA component was OOA (63% of OA mass
11 on average). HOA related to traffic emissions contributed on a yearly average 17% to the OA
12 mass, while COA was a minor source contributing 4%. The contribution of INDOA was
13 enhanced during winter (17% during winter and 11% during summer), consistent with an
14 increased contribution from light alkanes, light PAHs (fluoranthene, pyrene, phenantrene) and
15 selenium, which is commonly considered as an unique coal combustion and coke production
16 marker. Online- and offline-AMS source apportionments revealed evolving
17 levoglucosan:BBOA ratios, being higher during late autumn and March. A similar seasonality
18 was observed in the ratios of cellulose combustion markers to lignin combustion markers,
19 highlighting the contribution from cellulose rich biomass combustion, possibly related to
20 agricultural activities.

21

22 **1 Introduction**

23 Outdoor particulate air pollution is estimated to be responsible for approximately 3.3 million
24 premature deaths each year worldwide, and this number is projected to double by 2050
25 (Lelieveld et al., 2015). Organic aerosols (OA) can contribute up to 90% of the PM₁ (Jimenez
26 et al., 2009), therefore understanding their main emission sources and formation processes is a
27 key prerequisite for the development of appropriate mitigation policies.

28 In the Mediterranean basin, sources and trends of OA remain scarcely investigated, despite
29 their deleterious impact in such a densely populated region. The Mediterranean region is
30 characterized by an intense photochemistry during summer. Not surprisingly, the majority of
31 the OA source apportionment studies conducted in the region using aerosol mass
32 spectrometry (AMS) focused on the summer period (e.g., El Haddad et al., 2013; Minguillón

1 et al., 2011, 2016; Hildebrandt et al., 2011). Through positive matrix factorization (PMF)
2 techniques, these studies revealed that during summer the oxygenated organic aerosol (OOA)
3 fraction formed by oxidation of gaseous precursors, represented the largest part of OA.
4 Amongst these studies, the field deployment of the AMS in Marseille, the largest port in the
5 Mediterranean, has demonstrated that this instrument is well suited for quantifying the
6 contribution of industrial emissions (El Haddad et al., 2013). In that work, the industrial OA
7 factor was identified by the high correlation with heavy metals and AMS-polycyclic aromatic
8 hydrocarbons (AMS-PAHs), moreover strong increments of the industrial factor
9 concentrations were systematically observed when winds shifted to the west/south west,
10 consistent with back-trajectory analysis highlighting the transport of industrial emissions from
11 an industrial pole. Overall the industry-related OA contributed on average 7% of the bulk OA
12 mass (El Haddad et al., 2011; 2013). However, these results were limited to 2 weeks of
13 measurements during summer while the contribution of industrial emissions during the rest of
14 the year remains unknown.

15 There is a general paucity of AMS and ACSM datasets in the Mediterranean region during
16 winter. Exceptions include AMS campaigns (Mohr et al. 2012; Hildebrandt et al., 2011)
17 covering a few weeks during late winter-early spring, and studies with an aerosol chemical
18 speciation monitor (ACSM) (e.g., Minguillón et al., 2015, covering three weeks of
19 monitoring). The measurement of organic markers and elements (e.g., Salameh et al., 2015;
20 Reche et al., 2012) at different stations indicate a substantial contribution from biomass
21 burning (BB). However, the sources and chemical composition of this fraction and its
22 evolution during the year remain uncertain. Modelling results within the European Monitoring
23 and Evaluation Programme (EMEP) have shown that the South of France, together with
24 Portugal, can be a major hot spot in Europe for OA during February-March, possibly due to
25 agricultural fires (Dernier van der Gon et al., 2015; Fountoukis et al., 2014). In this region,
26 BBOA can derive from various processes such as agricultural land clearing activities,
27 wildfires, and domestic heating, and therefore may have a variable chemical composition.

28 The current study capitalizes on the AMS measurements of offline samples collected over one
29 year (2011-2012), in Marseille, an ideal environment for the characterization of urban
30 emissions from biomass burning, traffic and industrial activities and their transformation
31 under high photochemical activity. The source apportionment results obtained from PMF
32 applied to the OA mass spectra are corroborated using a comprehensive set of offline

1 measurements including elemental and organic carbon (EC/OC) measurements, as well as
2 measurements of elements by inductively coupled plasma mass spectrometry (ICP-MS), of
3 molecular markers by gas chromatography mass spectrometry (GC-MS) and ultra-
4 performance liquid chromatography mass spectrometry (UPLC-MS), and of major ions by ion
5 chromatography (IC). We mainly focus on the sources and trends of winter OA and therefore
6 we additionally analyzed an online AMS dataset acquired at the same location during the
7 winter of the previous year. The comparison of online- and offline-AMS data, and organic
8 marker concentrations enables an in-depth characterization of OA sources in Marseille, and in
9 particular the identification of the main processes by which biomass smoke is emitted and
10 transformed in this region.

11

12 **2 Methods**

13 **2.1 Site description**

14 Marseille is the second largest city in France with more than 1 million inhabitants (2010). It
15 hosts the largest harbor in France and in the Mediterranean Sea. Many port-related industries,
16 especially petrochemical companies, are located in a big cluster. These facilities are situated
17 about 40 km NW from the city and include steel facilities, coke production plants, oil storing,
18 refining plants, and several shipyards. The Marseille commercial harbor is located in the
19 vicinity of this industrial cluster and represents the third-largest harbor of the world for crude
20 oil storage and treatment. During summer, typical wind patterns in the city of Marseille favor
21 the transport of polluted air masses from the industrial cluster to the city, including the sea
22 breeze and the light Mistral wind from the Rhone valley. At night, the land breeze may
23 transport air masses from an agricultural valley located east of the sampling site. A more
24 detailed description of wind patterns in Marseille can be found in Drobinski et al. (2007) and
25 Flaounas et al. (2009). The sampling location is classified as an urban background station and
26 is situated in the urban park “Cinq Avenue” in a traffic-free zone near the city center
27 (43°18'20'' N, 5°23'40''E; 64 m a.s.l.).

1 **2.2 Yearly cycle dataset**

2 *Sample collection.*

3 In total, 216 24-h (from midnight-to-midnight) integrated PM_{2.5} pre-baked (500°C for 3 h)
4 quartz fiber filters (150 mm diameter, Tissuquartz) were collected between 30 July 2011 and
5 20 July 2012 using a High-Volume sampler (Digitel DA80) operated at 500 L min⁻¹ (Batch 1).
6 Filter samples were subsequently wrapped in aluminum foil, sealed in polyethylene bags and
7 stored at -18°C.

8 *Offline-AMS analysis.* This work discusses the offline-AMS analysis of 55 composite samples
9 (created from the batch of 216 PM_{2.5} filters collected) which were analyzed by Salameh et al.
10 (*submitted*) for major ions, molecular markers and elements (Table S1). A thorough
11 description of the offline-AMS analysis can be found in Daellenbach et al. (2016). One punch
12 per filter sample (from 5 to 25 mm diameter depending on the filter loading and on the
13 number of punches per composite sample) was prepared for analysis. Punches from the same
14 composite sample were extracted together in 15 mL of ultrapure water (18.2 MΩ cm, total
15 organic carbon < 5ppb, 25°C) in an ultrasonic bath for 20 min at 30°C. After extraction, filters
16 were vortexed for 1 min, and the resulting liquids were filtered with 0.45 μm nylon membrane
17 syringe filters.

18 The generated liquid extracts were atomized in air using a custom-made two-nozzle nebulizer.
19 The generated aerosol was dried using a silica gel diffusion drier and then measured by a high
20 resolution time-of-flight AMS (HR-ToF-AMS, running in V-mode). In the AMS, particles are
21 flash vaporized (600°C) and the resulting gas is then ionized by electron impact (EI, 70eV),
22 yielding quantitative mass spectra of the non-refractory submicron aerosol components,
23 including OA, NO₃⁻, SO₄²⁻, NH₄⁺, and Cl⁻. A detailed description of the AMS operating
24 principles, calibration protocols, and analysis procedures are provided by DeCarlo et al.
25 (2006). In total about 10 mass spectra (mass range 12-300 Da, 60 sec averaging time) were
26 collected per composite sample. Between each sample, a measurement blank was recorded via
27 nebulization of ultra-pure water to minimize and monitor the possible memory effects of the
28 system. In total five mass spectra were collected per each measurement blank. Offline-AMS
29 data were processed and analyzed using the HR-ToF-AMS analysis software SQUIRREL
30 (SeQUential Igor data RetRiEvaL) v.1.52L and PIKA (Peak Integration by Key Analysis)
31 v.1.11L for IGOR Pro software package (Wavemetrics, Inc., Portland, OR, USA). HR

1 analysis of the mass spectra was performed in the mass range 12-115 Da and in total 217 ion
2 fragments were fitted.

3 The interference of NH_4NO_3 on the CO_2^+ signal was corrected according to Pieber et al.
4 (2016) as follows:

$$5 \quad CO_{2,real} = CO_{2,meas} - \left(\frac{CO_{2,meas}}{NO_{3,meas}} \right)_{NH_4NO_3,pure} * NO_{3,meas} \quad (1)$$

7 where the $\left(\frac{CO_{2,meas}}{NO_{3,meas}} \right)_{NH_4NO_3,pure}$ correction factor was 2.5% as determined from aqueous
8 NH_4NO_3 measurements conducted regularly during the measurement period.

9 *Other offline measurements.* A complete list of the measurements performed can be found in
10 Table S1. To summarize, major ions (Ca^{2+} , Mg^{2+} , K^+ , Na^+ , NH_4^+ , NO_3^- , SO_4^{2-} , Cl^- , oxalate,
11 malate, succinate, and malonate) were measured by ion chromatography (IC) according to the
12 methodology described by Jaffrezo et al. (1998). A subset of the filters was selected for CO_3^{2-}
13 quantification following the method described by Karanasiou et al. (2011). The method
14 encompasses the fumigation of the filter samples with HCl. The CO_2 evolved by this
15 acidification of the carbonates deposited on the filters is detected by thermal optical
16 transmittance determination. The CO_3^{2-} measurements agreed fairly well with the CO_3^{2-}
17 estimate from ion balance calculations based on IC data (Fig. S1). In the following discussion,
18 ion concentrations from filter samples always refer to the IC measurements unless otherwise
19 specified.

20 Elemental and organic carbon (EC and OC) were determined for each filter by thermal optical
21 transmittance using a Sunset Lab analyzer (Birch and Cary, 1996) following the EUSAAR2
22 protocol (Cavalli et al., 2010). The CO_3^{2-} concentration determined from the IC ion balance
23 was then subtracted from OC concentration. The water soluble OC (WSOC) was measured
24 with a total organic carbon analyzer (TOC) following the methodology described in Bozzetti
25 et al. (2016a) and references therein. Before the analyses, the liquid extracts were treated with
26 a 2 M HCl solution for 1-30 min to remove the inorganic C fraction. Total nitrogen (TN) was
27 determined using a TOC analyzer combustion tube. The NO_2 generated from the water
28 soluble (WS) N decomposition was detected by a chemiluminescence TNM-1 unit detector.
29 Organic markers were measured via GC-MS analysis, following the methodology described
30 in El Haddad et al. (2009; 2011), Favez et al. (2010) and Piot et al. (2012). In total 15
31 different polycyclic aromatic hydrocarbons (PAH), 19 alkanes (C19-C36), 8 hopanes, 5

1 phthalate esters, levoglucosan, 6 lignin pyrolysis compounds, 6 fatty acids, and 3 sterols were
2 determined (Table S1). 33 chemical elements (Table S1) were quantified using ICP-MS
3 according to the procedure described in Chauvel et al. (2010) and the modifications suggested
4 in El Haddad et al. (2011). A subset of 20 composite samples was selected for the
5 quantification of methyl-nitrocatechol isomers (Table S1) via Ultra Performance Liquid
6 Chromatography coupled with an Electro Spray Ionization – ToF - MS (UPLC-ESI-ToF-MS),
7 following the procedure described in Iinuma et al. (2010).

8 **2.3 Intensive winter campaign**

9 A HR-ToF-AMS was deployed at the same station (urban park “Cinq Avenue”) between 25
10 January 2011 and 2 March 2011 to monitor the real-time NR-PM₁ aerosol chemical
11 composition. Although February 2011 is not included in the sampling period covered by
12 offline-AMS, these online measurements nonetheless provide a good opportunity to compare
13 the separation, relative contributions and winter seasonal trends of the OA sources retrieved
14 by the offline- and online-AMS source apportionment procedures. Summer offline-AMS
15 results were instead compared with online-AMS source apportionment results reported by El
16 Haddad et al. (2013). The AMS was operated with an averaging time of 8 minutes, and in
17 total 5633 mass spectra were collected during the monitoring period. We performed an
18 ionization efficiency (IE) calibration by NH₄NO₃ nebulization, and the resulting IE value of
19 $1.76 \cdot 10^{-7}$ was applied to the dataset. The standard relative ionization (RIE) efficiency was
20 assumed for organics (1.4), SO₄²⁻ (1.2), NH₄⁺ (4) and Cl⁻ (1.3), while the collection efficiency
21 (CE) was estimated using the composition dependent collection efficiency model
22 (Middlebrook et al., 2012). Total AMS-PAHs were estimated from AMS data according to
23 Dzepina et al. (2007).

24 Similarly to offline-AMS, online-AMS data were also processed and analyzed using HR-ToF-
25 AMS Analysis software SQUIRREL (SeQUential Igor data RetRiEval) v.1.52L and PIKA
26 (Peak Integration by Key Analysis) v.1.11L for IGOR Pro software package (Wavemetrics,
27 Inc., Portland, OR, USA). HR analysis of the mass spectra was performed in the mass range
28 12-115 Da and in total 215 ion fragments were fitted.

29 A NO_x analyzer was run in parallel to the AMS to monitor the real-time NO_x concentration. A
30 set of pre-baked (500°C for 3h) 24-h integrated PM_{2.5} filter samples was also collected during
31 this campaign (Batch 2) following the same sampling and storage procedure described in

1 Section 2.2. Filters were analyzed for major ions, metals, elemental and organic carbon
 2 (EC/OC), and organic markers, including n-alkanes, hopanes, polyaromatic hydrocarbons
 3 (PAHs), lignin and cellulose pyrolysis products using the techniques previously described in
 4 Section 2.2 (Table S1).

5

6 Table 1. Monitoring periods.

Online-AMS	Offline-AMS
28 January 2011 – 02 March 2011	30 July 2011 – 20 July 2012

7

8 **2.4 Source apportionment**

9 *Implementation.* The online- and offline-AMS source apportionment results discussed in this
 10 work were obtained from PMF analysis (Paatero and Tapper, 1994) of AMS spectra using the
 11 Multilinear Engine (ME-2, Paatero 1999). The Source Finder toolkit (SoFi, Canonaco et al.,
 12 2013, v.5.1) for Igor Pro (Wavemetrics, Inc., Portland, OR, USA) served as interface for data
 13 input and results evaluation. PMF is a multilinear statistical tool used to describe the
 14 variability of a multivariate dataset as the linear combination of static factor profiles times
 15 their corresponding time series, as described in Eq. 2:

$$16 \quad x_{i,j} = \sum_{z=1}^p g_{i,z} \cdot f_{z,j} + e_{i,j} \quad (2)$$

17 Here $x_{i,j}$, $g_{i,z}$, $f_{z,j}$, and $e_{i,j}$ represent respectively elements of the data matrix, factor time series
 18 matrix, factor profile matrix and residual matrix, while subscripts i,j and z denote time
 19 elements, variables (in our case AMS fragments), and discrete factor numbers, respectively. p
 20 represents the total number of factors selected by the user for current given PMF solution. The
 21 PMF algorithm returns only $g_{i,z}$ and $f_{z,j}$ values ≥ 0 , and solves Eq. 2 by minimizing the object
 22 function Q , defined as:

$$23 \quad Q = \sum_i \sum_j \left(\frac{e_{i,j}}{s_{i,j}} \right)^2 \quad (3)$$

1 Here $s_{i,j}$ is an element of the error input matrix. PMF is subject to rotational ambiguity, i.e.
 2 different $\mathbf{G}\cdot\mathbf{F}$ combinations characterized by the same Q can exist. The ME-2 implementation
 3 of the PMF algorithm offers an efficient exploration of the solution space by directing the
 4 solution toward environmentally-meaningful rotations by constraining the factor profile
 5 elements $f_{z,j}$ for one or more z factors. In the a -value implementation of ME-2, the elements of
 6 the factor profile matrix \mathbf{F} (in our case AMS fragments) are forced to predefined values $f_{z,j}$
 7 allowing a certain variability defined by the a -value, such that the modelled element $f_{z,j}'$
 8 satisfies Eq. 4:

$$9 \frac{(1-a)f_{z,n}}{(1+a)f_{z,m}} \leq \frac{f_{z,n'}}{f_{z,m'}} \leq \frac{(1+a)f_{z,n}}{(1-a)f_{z,m}} \quad (4)$$

10 where n and m represent any two arbitrary variables in the normalized \mathbf{F} matrix. A complete
 11 description of the a -value approach can be found elsewhere (Canonaco et al., 2013).

12 For the offline-AMS source apportionment, the PMF input data matrix was constructed as
 13 follows: each composite sample is represented by approximately 10 time points i ,
 14 corresponding to the ~ 10 mass spectra collected per filter sample (section 2.4). Each point of
 15 the data matrix is subtracted by the average corresponding measurement blank.

16 The error matrices were instead constructed as follows. For online-AMS source
 17 apportionment, the error matrix elements $s_{i,j}$ were calculated according to Allan et al. (2003)
 18 and Ulbrich et al. (2009), and included the uncertainty deriving from electronic noise, ion-to-
 19 ion variability at the detector, and ion counting statistics. $s_{i,j}$ included also a minimum error
 20 which was applied according to Ulbrich et al. (2009). For the offline-AMS source
 21 apportionment, the error term $\delta_{i,j}$ was calculated in the same way, but a further term ($\sigma_{i,j}$)
 22 including the blank subtraction uncertainty was propagated according to Eq. 5:

$$23 \quad s_{i,j} = \sqrt{\delta_{i,j}^2 + \sigma_{i,j}^2} \quad (5)$$

24 Finally for both online- and offline-AMS we applied a down-weighting factor of 3 to all
 25 variables with an average signal to an average error ratio lower than 2 (Ulbrich et al., 2009).
 26 No variable with an average signal to error value lower than 0.2 was detected.

27 Dust and ash can contain significant amount of inorganic CO_3^{2-} . Both the IC balance and the
 28 CO_3^{2-} measurements revealed non-negligible contributions from CO_3^{2-} in the $\text{PM}_{2.5}$ fraction
 29 (Fig. S1). Preliminary PMF results also resolved a factor correlating with Ca^{2+} (SI) which was
 30 characterized by high $f\text{CO}_2^+$, suggesting a possible solubilisation of CO_3^{2-} from dust which

1 could affect the OA mass spectral fingerprint. Overall, as discussed in the SI, we could not
2 achieve a clear inorganic dust separation using PMF, therefore we opted for a correction of
3 the PMF input matrices. The measured pH of our filter extracts was never >8, therefore we
4 can exclude the presence of CO_3^{2-} in the extracts, but rather assume all solubilized CO_3^{2-} to
5 exist as HCO_3^- . Direct measurements of nebulized standard NaHCO_3 aqueous solutions,
6 revealed that thermal decomposition of HCO_3^- on the AMS vaporizer (600°C) releases CO_2
7 (Fig. S2). Currently no HCO_3^- correction for the OA spectra is implemented in the standard
8 AMS fragmentation table (Aiken et al., 2008), therefore the measured CO_2^+ signal needs to be
9 subtracted from the OA AMS spectra. Offline-AMS PMF input matrices were corrected for
10 HCO_3^- and rescaled for $\text{WSOM}_i (= \text{WSOC}_{\text{TOC}}(\text{OM:OC})_{\text{offline-AMS}})_i$ according to the procedure
11 described in the Supplementary information, SI.

12 *Online-AMS source apportionment optimization.* In the following we describe the
13 optimization of the online-AMS source apportionment results. In order to optimize the source
14 separation we performed sensitivity analyses on PMF solutions. We adopted different
15 optimization strategies for online- and offline-AMS source apportionments (SI) as we
16 encountered dissimilar mixings between sources. This is not surprising as the two methods are
17 characterized by different time resolution and different monitoring time extension (1 year for
18 offline-AMS, 1 month for online-AMS), which in turn result in different variabilities
19 apportioned by the PMF algorithm (daily for online-AMS vs. seasonal for offline-AMS).

20 In order to optimize the source separation, we performed sensitivity analyses on PMF
21 solutions according to the following scheme:

- 22 I) Selection of the number of factors based on residual analysis.
- 23 II) Qualitative evaluation of the unconstrained PMF solution in comparison with
24 the constrained PMF solutions (*a*-value approach: COA and/or HOA
25 constraints)
- 26 III) Constrain of both the HOA and COA factors profiles adopting an *a*-value
27 approach. *a*-value sensitivity analysis (121 PMF runs performed scanning all
28 the COA and HOA *a*-value combinations, *a*-value scanning steps: 0.1).
- 29 IV) Classification of the 121 PMF runs based on the cluster analysis of the COA
30 diurnal cycles. Selection of the best clusters, and corresponding PMF solutions.
- 31 V) PMF rotational ambiguity exploration. 100 bootstrap (Davison and Hinkley,
32 1997; Brown et al., 2015) PMF runs were performed by simultaneously

1 varying the COA and HOA a -value combinations (using only the optimal a -
2 value combinations identified from step IV). The average of the 100 bootstrap
3 runs represented the online-AMS source apportionment average solution. The
4 corresponding standard deviation represents the source apportionment
5 uncertainty.

6 For online-AMS we selected a 4-factor solution based on residual analysis. We investigated
7 the time dependent $Q(t)/Q_{exp}(t)$ evolution when increasing the number of factors. Q/Q_{exp} is
8 defined as the ratio between Q (as defined in Eq. 3) and the remaining degrees of freedom of
9 the model solution (Q_{exp}) calculated as $i \cdot j - (j+i)p$ (Canonaco et al., 2013). A decrease of the
10 Q/Q_{exp} , from lower to higher order solutions indicates an improvement in the variation
11 explained by the model. In particular we calculated the $\Delta(Q/Q_{exp}(t))$ obtained as the difference
12 between the $Q/Q_{exp}(t)$ for a (z)-factor solution minus the $Q/Q_{exp}(t)$ value obtained from the (z -
13 1)-factor solutions, where z indicates the number of factors. We observed a large reduction of
14 $\Delta(Q/Q_{exp}(t))$ until 4 factors (Fig. S4). Higher order solutions provided only minor
15 contributions to the explained variability and in terms of solution interpretability resulted in a
16 splitting of primary sources which could not be unambiguously associated to specific aerosol
17 sources or processes.

18 Using an a -value approach, we constrained HOA and COA profiles from Mohr et al. (2012)
19 and Crippa et al. (2013b) respectively. Leaving COA and/or HOA unconstrained enabled
20 resolving COA only by increasing the number of factors (>5 factor solutions) while in the 4
21 factor solutions we observed a splitting of an OOA factor which could not be attributed to
22 specific processes. Unconstrained PMF yielded HOA and COA time series well correlating
23 with the constrained solutions; however in the unconstrained case, HOA and COA factor
24 profiles showed higher $f\text{CO}_2^+$ in comparison with literature studies (Crippa et al., 2013b;
25 Mohr et al., 2012; Bruns et al., 2015; Docherty et al., 2011; Setyan et al., 2012; He et al.,
26 2010,) and in comparison with the constrained PMF runs. This in turn resulted in higher HOA
27 and COA concentrations, with background night concentrations 2-3 times higher than in the
28 constrained solutions, possibly indicative of mixings with oxidized aerosols (Fig. S5). Similar
29 differences between constrained and unconstrained PMF runs were also observed in Elser et
30 al. (2016). Also the HOA:NO_x ratio ($\mu\text{g m}^{-3}/\mu\text{g m}^{-3}$) matched typical literature values reported
31 for France (0.02 Favez et al., 2010) in the constrained PMF case (0.023), while for the
32 unconstrained approach it showed higher values (0.033).

1 For both offline- and online-AMS the constrained HOA profiles were from Mohr et al.
2 (2012), while the COA profiles were from Crippa et al. (2013b). The HOA profile from Mohr
3 et al. (2012) was selected for offline-AMS consistently with Daellenbach et al. (2016), since
4 the same factor recovery distributions were applied in this work. The same profile was
5 applied to online-AMS for consistency. Overall, as discussed in the SI, the HOA profiles from
6 literature showed high cosine similarities with each other, indicating that the AMS mass
7 spectral fingerprints from traffic exhaust are relatively stable from station to station and
8 consistent also with direct emission studies, making the selection of the constrained factor
9 profiles not crucial. More variability instead is observed among COA literature profiles. For
10 COA we selected the profile from Crippa et al. (2013b) which showed the lowest $f_{C_2H_4O_2^+}$
11 value among the considered ambient literature spectra (Crippa et al., 2013b; Mohr et al.,
12 2012). This guaranteed a better separation of COA from BBOA, as $C_2H_4O_2^+$ is strongly
13 related to levoglucosan fragmentation (Alfarra et al., 2007).

14 An a -value sensitivity analysis was performed by scanning all possible a -value combinations
15 for HOA and COA given by an a -value range 0-1 with a step size of 0.1. In order to optimize
16 the source apportionment results, we retained only the PMF solutions satisfying an acceptance
17 criterion described hereafter.

18 PMF factors were associated to specific aerosol emissions/processes based on mass spectral
19 features, diurnal cycles, and time series correlations with tracers. The identified factors were
20 associated to traffic (HOA), cooking (COA), biomass burning (BBOA), and oxygenated
21 organic aerosol (OOA). A thorough interpretation of the PMF factors will be discussed in the
22 Results section. Given the absence of widely accepted tracers for COA emissions, the
23 optimization of the COA contributions was based on the analysis of the COA diurnal cycles.
24 From the HOA and COA a -value sensitivity analysis we obtained a set of 121 PMF solutions
25 each one including both factor profiles and factor time series. PMF solutions obtained in this
26 way were categorized according to a cluster analysis of the normalized COA diurnal cycles
27 (Elser et al. 2016 and references therein). The k -means clustering approach enables
28 classifying the PMF solutions into k clusters, by minimizing a cost function (C):

$$29 \quad C = \sum_{i,z} ((x_i - \mu_{z,i})^2) \quad (6)$$

30 where C represents the sum of the Euclidian distances between each observation (x_i) and its
31 respective cluster centre ($\mu_{z,i}$), according to Eq. 6.

32 The number of clusters (k) that best represents the data is a critical choice in order to
33 perform a proper cluster analysis. The addition of a cluster ($k+1$) on one hand adds

1 complexity to the solution, while on the other hand decreases the cost function. A typical
2 strategy to select the right number of clusters is to explicitly penalize the addition of new
3 clusters by using Bayesian information criteria. This approach consists in adding a penalty
4 term to Eq. 6 proportional to the number of clusters (k):

$$5 \quad C' = \sum_{i,z} ((x_i - \mu_{z,i})^2) + k \cdot \ln(D) \quad (7)$$

6 where D denotes the dimensionality of the clusters (24 in our case, as we consider diurnal
7 cycles with hourly time resolution). In this study the C' function showed the minimum at 5
8 clusters (Fig. S6). The absence of convexity properties (i.e. several local minima can exist and
9 the solution strongly depends on the initialization) represents a possible drawback of the k -
10 means algorithm, therefore 100 random initializations of the k -means algorithm were
11 conducted.

12 The best clusters are selected based on a novel statistical analysis of the HOA, COA and
13 BBOA average cluster spectra (SI). Briefly, a cluster was retained if the HOA, COA, and
14 BBOA average cluster spectra were not statistically different from the average reference
15 HOA, COA, and BBOA spectra from literature (Crippa et al., 2013b; Mohr et al., 2012; Bruns
16 et al., 2015; Docherty et al., 2011; Setyan et al., 2012; He et al., 2010, Table S3). A complete
17 description of the best clusters selection is reported in the SI (Figs. S6-S10). Overall, three
18 clusters were retained and 2 were rejected. Finally, we retained only the PMF solutions that
19 were attributed to the 3 best clusters in more than 95% of the k -means random initializations
20 (Fig. S9).

21 In order to explore the rotational ambiguity of our PMF model we performed 200 PMF runs
22 by initiating the PMF algorithm using different input matrices. The 200 different input
23 matrices were generated using a bootstrap approach (Davison and Hinkley, 1997; Brown et
24 al., 2015). In short, the bootstrap approach creates new input matrices by randomly
25 resampling mass spectra (i elements) from the original input matrices. Note that some mass
26 spectra are resampled multiple times, while others are not represented at all. On average we
27 randomly resampled $63 \pm 1\%$ of the original spectra per bootstrap PMF run. Finally, each
28 bootstrap PMF run was initiated by randomly varying the HOA and COA a -values using the
29 $\{a\text{-value HOA}; a\text{-value COA}\}$ combinations previously selected as optimal from the cluster
30 analysis (Fig. S10). Only solutions showing a higher COA diurnal correlation with the three
31 selected clusters than with the two rejected clusters were retained. In this way we rejected
32 3.7% of the solutions. In the following we present the average bootstrap solution. The source
33 apportionment uncertainty is calculated as the variability of the retained bootstrap PMF runs.

1

2 *Offline-AMS source apportionment optimization.*

3 In this section we discuss the optimization of the offline-AMS source apportionment. The
4 PMF input matrices included 217 ions and 538 time elements deriving from about 10 AMS
5 mass spectral repetitions collected for each of the 54 composite samples.

6 In order to optimize the source separation, we performed sensitivity analyses on PMF
7 solutions according to the following scheme:

8 I) Selection of the number of factors based on residual analysis.

9 II) Qualitative evaluation of the unconstrained PMF solution in comparison with
10 the constrained PMF solutions (*a*-value approach: COA and/or HOA
11 constraints)

12 III) PMF rotational ambiguity exploration. 1080 bootstrap (Davison and Hinkley,
13 1997; Brown et al., 2015) PMF runs were performed by simultaneously
14 varying the COA and HOA *a*-value combinations. PMF solutions were
15 retained based on the correlation of the PMF factors with external tracers. The
16 PMF solutions retrieved from this step are relative to the water-soluble
17 fraction. The corresponding water-soluble OC factor concentrations were
18 determined by dividing the water-soluble OM factor concentrations (PMF
19 output) by the OM:OC ratio determined from the corresponding factor mass
20 spectrum.

21 IV) Retained water-soluble OC PMF solutions from step (III) were rescaled to the
22 total OC concentrations by applying factor recoveries. Factor recoveries were
23 fitted (using *a*-priori information) to match total OC. Only PMF solutions and
24 factor recoveries fitting OC with yearly and seasonally homogenous residuals
25 were retained. The average of the retained PMF solutions represented the
26 average source apportionment results. The corresponding standard deviation
27 represented the source apportionment uncertainty.

28 Based on analysis of the PMF residuals, we selected a 5-factor solution to explain the
29 variability of our dataset (Fig. S11). Similar to online-AMS, we monitored the decrease in
30 Q/Q_{exp} when increasing the number of factors (*z*). In this study, a large Q/Q_{exp} decrease was
31 observed until 5 factors. We also observed a clear $\Delta Q/Q_{exp}$ structure removal until 5 factors,
32 with higher order solutions leading to additional factors that were not attributable to specific

1 aerosol sources/processes. The 5 separated factors included HOA, COA, BBOA, OOA, and
2 industry-related OA (INDOA). The complete validation of the PMF factors will be discussed
3 in the Results section.

4 As already mentioned, the HOA and COA profiles were constrained using an a -value
5 approach. Consistently with online-AMS we constrained the profiles according to Mohr et al.
6 (2012) and Crippa et al. (2013b) respectively. Unconstrained PMF runs for offline-AMS did
7 not resolve HOA and COA factors. To explore the rotational ambiguity of our PMF model we
8 performed 1080 bootstrapped PMF runs. In this case we performed a higher number of
9 bootstrap runs than online-AMS because the COA and HOA a -value combinations could not
10 be separately optimized because the offline-AMS method cannot resolve diurnal patterns.
11 Each PMF run was also initiated using different input matrices. As previously mentioned the
12 input matrices contained about 10 mass spectral repetitions per filter sample, therefore the
13 bootstrap algorithm was implemented to randomly resample 54 filters samples, each one with
14 all the corresponding mass spectral repetitions. The final generated matrices included 54
15 samples; note that some filter samples could be resampled more times, while others were not
16 resampled at all. On average $63 \pm 5\%$ of the original samples were resampled. Finally, each of
17 the PMF runs was initiated by randomly varying the HOA and COA a -values. The optimal
18 PMF solutions were selected based on 6 acceptance criteria including:

- 19 1) Significantly ($p=0.05$) positive Pearson correlation coefficient R between BBOA and
20 levoglucosan.
- 21 2) Significantly positive R between HOA and NO_x .
- 22 3) Significantly positive R between INDOA and Se.
- 23 4) BBOA correlation with levoglucosan (R) significantly higher than the correlation
24 between COA and levoglucosan.
- 25 5) HOA correlation with NO_x significantly higher than the correlation between COA and
26 NO_x .
- 27 6) COA correlation with Se significantly smaller than the correlation between INDOA
28 and Se.

29 Criteria 1-3 analyse the correlation between factor and marker time series. The significance of
30 a correlation was determined by calculating the Fisher transformed correlation coefficient z
31 (Garcia, 2011):

$$z = 0.5 * \ln\left(\frac{1+R}{1-R}\right) = \arctan(R) \quad (8)$$

where R is the Pearson correlation coefficient between factor and marker time series. Subsequently we conducted a t -test to verify the significance ($\alpha=0.95$) of the correlation:

$$t = \frac{R}{\sqrt{\frac{1-R^2}{N-2}}} \quad (9)$$

Here, N represents the number of samples (54). For a confidence interval of 95% the minimum significant correlation was $R = 0.23$. For criteria 4-6, in order to evaluate whether HOA, BBOA and INDOA correlated significantly better than COA with their corresponding markers, we compared the z values obtained between each factor and its corresponding tracer (e.g. BBOA and levoglucosan) and between COA and the same tracer (e.g. levoglucosan), using a standard error on the z distribution of $1/\sqrt{N-3}$ (Zar, 1999).

In total, we retained 1.5% of the PMF runs. The criteria that discarded the largest number of solutions were the ones based on COA (4-6) correlation with tracers of other sources. This suggests that for this dataset the COA separation from other sources was particularly difficult due to the absence of high temporal resolved data which aids the separation of a distinct COA diurnal cycle. Moreover, this separation is also complicated by the small COA contribution estimated by both online- and offline-AMS source apportionments (on average $0.4 \mu\text{g m}^{-3}$ as discussed in the following sections). Furthermore, the relatively small COA factor recovery (R_{COA} median 0.54) hampers the COA apportionment by offline-AMS.

The PMF performed on offline-AMS mass spectra returned water-soluble OA factor concentrations, $WSKOA_i$. To rescale the water-soluble OA concentration to the total OA, KOA_i , we used the factor recoveries (R_k) reported by Daellenbach et al. (2016) for the HOA, COA, BBOA, and OOA factors (R_{HOA} , R_{COA} , R_{BBOA} , R_{OOA}).

$$KOA_i = WSKOA_i/R_{KOA} \quad (10)$$

This is the first offline-AMS study where an INDOA factor was identified. Therefore, we determined the INDOA recovery (R_{INDOA}) in this study, by performing a single parameter fit according to Eq. 11:

$$OC_i = \frac{WSHOA_i}{\frac{\partial M}{\partial C_{HOA}} \cdot R_{HOA}} + \frac{WSCO A_i}{\frac{\partial M}{\partial C_{COA}} \cdot R_{COA}} + \frac{WSBBOA_i}{\frac{\partial M}{\partial C_{BBOA}} \cdot R_{BBOA}} + \frac{WSOOA_i}{\frac{\partial M}{\partial C_{OOA}} \cdot R_{OOA}} + \frac{WSINDOA_i}{\frac{\partial M}{\partial C_{INDOA}} \cdot R_{INDOA}} \quad (11)$$

1 500 different fits were performed for each of the retained PMF solutions. Moreover each fit
2 was initiated using different R_{KOA} combinations randomly selected from the R_{KOA}
3 combinations determined by Daellenbach et al. (2016) and reported in Bozzetti et al. (2016a).
4 In order to account for possible WSOC and OC systematic measurement biases, each fit was
5 initiated by also perturbing the OC_i , $WSKOA_i/(OM:OC)_{WSKOC}$, and R_{KOA} inputs assuming for
6 each parameter a possible bias of 5%, corresponding to the WSOC and OC measurement
7 accuracy (we note that the sum of the $WSKOC_i/(OM:OC)_{WSKOC}$ terms equals $WSOC_i$ neglecting the
8 PMF residuals). Finally the input OC_i was randomly perturbed within its measurement
9 uncertainty assuming a normal distribution of the errors. Among the performed fits we
10 retained the recovery combinations and factor time series associated with OC_i unbiased
11 residuals (residual distribution centered on 0 within the 1st and 3rd quartiles) for all seasons
12 together and for summer and winter separately (Fig. S12). Accordingly, we retained 13% of
13 the solutions. All the retained factor recovery combinations can be found at
14 <http://doi.org/10.5905/ethz-1007-75>. The median INDOA recoveries were estimated as 0.69
15 (1st quartile 0.65, 3rd quartile 0.73, Fig. S13), while the retained R_{KOA} for the other sources
16 were consistent within the quartiles with the R_{KOA} values reported by Daellenbach et al.
17 (2016) despite their input value was perturbed as described above. The variability of the
18 retained solutions is considered as our best estimate of the source apportionment uncertainty,
19 which accounts for offline-AMS repeatability, model rotational uncertainty explored
20 bootstrapping the input matrices and scanning the HOA and COA α -value sensitivity, and
21 R_{KOA} uncertainties. Overall, for a generic factor KOA, we estimated the corresponding
22 average relative uncertainty as follows: we calculated the campaign averages of the KOA
23 concentrations for each of the ν retained PMF solutions (\overline{KOA}_ν). The relative uncertainty of
24 the KOA concentration was calculated as the standard deviation of \overline{KOA}_ν divided by its
25 average.

26 We also explored a 4-factor solution without constraining the COA profile. In this case we
27 performed 100 bootstrap PMF runs by randomly varying the HOA α -value. Results revealed
28 the COA separation (in the 5-factor solution with COA constrained) affected the HOA
29 separation more than the other factors (BBOA, OOA, INDOA). Overall, when comparing the
30 4- and 5-factor solutions (without and with COA constrained, respectively) HOA showed not
31 statistically different concentrations within our estimated source apportionment uncertainty
32 for 85% of the samples, BBOA and OOA for 96%, and INDOA for 94%. This is probably due

1 to the high similarity between COA and HOA spectra (SI, “Best cluster selection” Section),
2 which are both characterized by high contributions from hydrocarbons.

3

4 **3 Source apportionment validation**

5 Figure 1 displays the stacked seasonal average concentrations of the measured PM_{2.5}
6 components (ions measured by IC, elements measured by ICP-MS, EC by the EUSAAR
7 method, and OM estimated as the sum of the offline-AMS PMF factors). Higher
8 concentrations were observed during winter than in summer due to the enhanced contributions
9 of NO₃⁻ and OM. NO₃⁻ increased during winter and autumn due to NH₄NO₃ partitioning into
10 the particle phase at lower temperatures. OM concentrations were higher during winter due to
11 the strong BBOA contributions.

12 Overall OM was the dominant PM_{2.5} component over the whole year highlighting the
13 importance of studying its sources. OM represented 46% of the total mass with higher relative
14 contributions during winter (51%) than in summer (37%). SO₄²⁻ represented the second most
15 abundant PM_{2.5} component, contributing on average 12% of the mass. Among the other
16 components, EC contributed 9% of the mass, NO₃⁻ 9% (13%_{avg} during winter and 3%_{avg}
17 during summer), NH₄⁺ 8%, the sum of the elements 7% (3% during winter and 13% during
18 summer, possibly because of dust resuspension), CO₃²⁻ 6%, Ca²⁺ 2%. K⁺, Cl⁻, Na⁺, and Mg²⁺
19 individually did not exceed 1% of the mass. In the following, subscripts *avg*, and *med* denote
20 average and median values, respectively.

21 **3.1 Online-AMS source apportionment validation**

22 PMF factors were associated to aerosol sources/processes based on mass spectral features
23 (Fig. 2), correlation with tracers (Fig. 3), and diurnal cycles (Fig. 4). The HOA was well-
24 correlated with NO_x ($R=0.86$), with peaks during rush hours (centered on 8h and 19h) and
25 higher concentrations during the first half of the campaign. The average HOA:NO_x ratio (μg
26 $\text{m}^{-3}/\mu\text{g m}^{-3}$) was 0.023, consistent with Favez et al. (2010). The COA diurnal variation showed
27 two peaks at lunch and dinner time (12.00 and 21.00), as observed in other cities (Elser et al.,
28 2016; Mohr et al., 2012). The BBOA factor profile showed the highest $f\text{C}_2\text{H}_4\text{O}_2^+$ and
29 $f\text{C}_3\text{H}_5\text{O}_2^+$ contributions among the apportioned factors. Previous studies (Alfarra et al., 2007)
30 associated the high $f\text{C}_2\text{H}_4\text{O}_2^+$ and $f\text{C}_3\text{H}_5\text{O}_2^+$ contributions in BBOA AMS spectra to the
31 fragmentation of anhydrous sugars from cellulose pyrolysis. The BBOA time series was well-

1 correlated with levoglucosan ($R=0.74$) and AMS-PAHs ($R=0.88$). Note that AMS-PAHs are
2 not unique BBOA tracers, but in general they derive from combustion sources (see SI for the
3 comparison between AMS-PAHs and GC-MS PAHs). In this specific dataset they could
4 partially derive from traffic, although from the AMS-PAHs multilinear regression, we
5 estimated that 79% of the AMS-PAHs are related to BBOA and 21% to HOA, indicating that
6 BBOA dominates the PAH emissions. The AMS-PAHs:HOA ratio was 0.0020, while the
7 AMS-PAHs:BBOA was 0.0028.

8 In general, industrial emissions can be an important source of PAHs at this location as
9 discussed in El Haddad et al. (2013). In presence of an industrial contribution, the BBOA vs.
10 AMS-PAHs correlation would decrease. In this work the correlation between AMS-PAHs and
11 the $C_2H_4O_2^+$ fragment, typically related to levoglucosan fragmentation (Alfarra et al., 2007),
12 was high ($R=0.87$) and no AMS-PAHs spike was observed without a simultaneous increase of
13 $C_2H_4O_2^+$ (Fig. S15). Moreover the industrial-related OA factor resolved by El Haddad et al.
14 (2013) was clearly associated to wind directions from W/SW (225° - 270°), while in this work
15 wind directions were oriented from W/SW only for 7% of the monitoring time, furthermore
16 without being associated to any significant increase in the AMS-PAHs concentration (Fig.
17 S16), indicating the absence of clear industrial episodes.

18 The BBOA diurnal cycle, similarly to AMS-PAHs, showed higher values at night than during
19 the day (Fig. 4). In addition, the BBOA highest concentrations were detected at night and
20 associated to slow wind speeds from the E/NE which is consistent with the night land breeze
21 direction. Moreover, strong enhancements of the BBOA factor concentrations were perceived
22 when the wind direction shifted to the E/NE (typically around 18 o'clock during the
23 monitoring period) suggesting that BBOA could be transported from the valleys nearby
24 Marseille (Fig. S18).

25 We calculated the BBOC time series by dividing the BBOA concentrations by the
26 OM:OC_{BBOA} ratio calculated from the average BBOA HR spectrum (1.60). The average
27 BBOC:levoglucosan ratio [$\mu\text{g m}^{-3}/\mu\text{g m}^{-3}$] was 0.15, comparable to other European studies
28 (Zotter et al., 2014; Herich et al., 2014; Minguillón et al., 2011).

29 The OOA profile showed the most oxidized mass spectral fingerprint with an O:C ratio of
30 0.67 in comparison to the values of 0.35 retrieved for BBOA, 0.12 for COA and 0.03 for
31 HOA. The OOA time series was well correlated with the NH_4^+ time series ($R=0.86$),
32 suggesting a probable secondary origin of the OOA factor (Lanz et al., 2008). The OOA

1 diurnal cycle was flat, suggesting OOA to be representative of regionally-transported
2 oxygenated aerosols, consistent with the conclusions of El Haddad et al. (2013).

3 **3.2 Offline-AMS source apportionment validation**

4 PMF factors from the offline-AMS dataset were related to aerosol sources/processes based on
5 mass spectral features (Fig. 5), seasonal trends and correlation with tracers (Fig. 6). A
6 comparison of the online-AMS and offline-AMS factor profiles is reported in the SI. In the
7 following, for a generic k factor, we calculated the corresponding KOC_i time series dividing
8 KOA_i by the OM:OC ratio determined from the average HR-AMS factor profile.

9 During summer, when biomass burning contributions to EC are low, HOA correlated well
10 with EC ($R = 0.76$) and yielded an HOC:EC (Hydrocarbon-like OC = $HOA/(OM:OC)_{HOA}$)
11 ratio of 0.64, similar to other European studies (El Haddad et al., 2009 and references
12 therein). Over the whole year, the retained PMF solutions showed an HOA correlation with
13 NO_x (R) spanning between 0.23 and 0.49. These low correlations are comparable to the ones
14 found by El Haddad et al. (2013) at the same station by online-AMS. In this case, the
15 relatively low HOA correlation with NO_x is probably due to the low R_{HOA} (median 0.11)
16 which together with the low HOA concentration ($1.5 \mu\text{g m}^{-3}_{avg}$, Results section), results in
17 small water-soluble HOA concentrations, leading to an uncertain HOA apportionment. This
18 was already reported in previous offline-AMS studies (Daellenbach et al., 2016; Bozzetti et
19 al., 2016a). Although the HOA variability could not be well captured, the estimated HOA
20 concentration was corroborated by the average HOA/NO_x ($0.02 \mu\text{g m}^{-3}/\mu\text{g m}^{-3}$) which was
21 found to be consistent with El Haddad et al. (2013) for the same station and with Favez et al.
22 (2010) for an alpine location in France.

23 BBOA was identified from its mass spectral features, with the highest $f_{C_2H_4O_2^+}$ and $f_{C_3H_5O_2^+}$
24 contributions among the apportioned factors, consistent with the findings of Alfarra et al.
25 (2007). BBOA correlated well with biomass combustion tracers measured by GC-MS, such as
26 levoglucosan ($R=0.76$), acetosyringone ($R=0.71$) and vanillic acid ($R=0.84$). The winter
27 average levoglucosan:BBOC [$\mu\text{g m}^{-3}/\mu\text{g m}^{-3}$] ratio was equal to 0.12, consistent with other
28 studies in Europe (Zotter et al., 2014; Herich et al., 2014; Minguillón et al., 2011).

29 The fourth factor (INDOA) was related to industrial emissions due to the high correlation
30 with light alkanes ($C_{19}-C_{22}$, $0.77 \leq R \leq 0.86$), Se ($R=0.54$), Pb ($R=0.44$) and with some PAHs

1 such as pyrene ($R=0.74$), fluoranthene ($R=0.77$), and phenanthrene ($R=0.74$). Among the
2 measured PAHs, pyrene, fluoranthene and phenanthrene showed the lowest correlations with
3 levoglucosan (Table S1, $R = 0.31, 0.29, \text{ and } 0.27$ respectively), suggesting that these
4 particular PAHs were overwhelmingly emitted by INDOA rather than BBOA. We note that
5 phenanthrene, pyrene, and fluoranthene together represent $9.6\%_{\text{avg}}$ of the PAHs mass
6 quantified by GC-MS, indicating that PAHs are overwhelmingly emitted by BBOA. While Se
7 is considered to be a unique coal marker in the literature (Weitkamp et al., 2005; Park et al.,
8 2014), in Marseille this source is likely related to coke and steel production facilities (El
9 Haddad et al., 2011). The average INDOA OM:OC (1.60) was intermediate between the
10 OM:OC ratios of HOA (1.23) and COA (1.28), and those of BBOA (1.85) and OOA (1.82).
11 El Haddad et al. (2013) resolved an industrial OA factor at the same station by online-AMS
12 PMF. In that work the authors suggested a probable contribution of oxygenated OA to the
13 resolved industrial factor, probably deriving from (photo)chemical aging during the transport
14 from the industrial facilities to the receptor site occasionally accompanied by new particle
15 formation processes within the industrial plume (as observed by the increased ultrafine
16 particle number concentration associated to W/SW wind directions). Considering the average
17 wind speed from W/SW (0.8 km/h), and the distance between the receptor site and the
18 Marseille commercial harbor (~ 40 km) we estimate an aging time of several hours, which
19 could lead to a more oxidized fingerprint in comparison to the fresh primary emissions
20 (Huang et al., 2014). Overall this factor explained the largest fraction of the variability of S-
21 and Cl-containing organic fragments such as C_2HSO^+ , CH_2SO^+ , CH_3Cl_2^+ , CH_4SO_3^+ ,
22 $\text{C}_3\text{H}_3\text{SO}_2^+$, and $\text{C}_7\text{H}_{16}^+$.

23 The last factor was defined as OOA as it showed a highly oxygenated fingerprint with the
24 largest CO_2^+ fractional contributions ($f\text{CO}_2^+$) among the apportioned factors (14%, in
25 comparison with 11% for BBOA, 2% for HOA, and 1% for COA and INDOA). This factor
26 showed on average the largest contributions over the year. Overall, the OOA: NH_4^+ ratio was
27 2.3_{avg} , in line with the values reported by Crippa et al. (2014) for 25 different European sites
28 (2.0_{avg} ; minimum value 0.3; maximum 7.3).

29 Previous offline-AMS (Bozzetti et al., 2016a; Bozzetti et al., 2016b; Daellenbach et al., 2016)
30 and online-ACSM studies (e.g., Canonaco et al., 2015) conducted in Switzerland and
31 Lithuania reported the separation of two OOA factors characterized by different seasonal
32 trends and different $\text{C}_2\text{H}_3\text{O}^+:\text{CO}_2^+$ ratios. In particular, the OOA factor characterized by the

1 highest $C_2H_3O^+ : CO_2^+$ ratio contributed mostly during summer and was linked to secondary
 2 OA from biogenic emissions. Here we calculated a $(C_2H_3O^+ : CO_2^+)_{OOA}$ ratio by subtracting the
 3 $C_2H_3O^+$ and CO_2^+ contributions deriving from primary sources, from the measured $C_2H_3O^+$
 4 and CO_2^+ (Canonaco et al., 2015):

$$5 \quad \frac{C_2H_3O^+}{CO_2^+}_{OOA,i} = \frac{C_2H_3O^+_{meas,i} - HOA_i \cdot f_{C_2H_3O^+_{HOA}} - BBOA_i \cdot f_{C_2H_3O^+_{BBOA}} - INDOA_i \cdot f_{C_2H_3O^+_{INDOA}} - COA_i \cdot f_{C_2H_3O^+_{COA}}}{CO_2^+_{meas,i} - HOA_i \cdot f_{CO_2^+_{HOA}} - BBOA_i \cdot f_{CO_2^+_{BBOA}} - INDOA_i \cdot f_{CO_2^+_{INDOA}} - COA_i \cdot f_{CO_2^+_{COA}}} \quad (12)$$

6 Overall, $C_2H_3O^+_{OOA}$, and $CO_2^+_{OOA}$ did not show a clear seasonality (Fig. S19), which
 7 hampered the separation of two OOA sources. Even though another OOA factor was not
 8 separated, El Haddad et al. (2013) estimated for the same location during summer a
 9 substantial contribution of secondary biogenic aerosol using ^{14}C measurements (no
 10 measurements conducted in other seasons). As a consequence the OOA factor resolved in this
 11 work explains both secondary biogenic and aged/secondary anthropogenic sources. The
 12 absence of a clear increase in the $(C_2H_3O^+ : CO_2^+)_{OOA}$ ratio in Marseille during summer could
 13 be explained by the large emissions of anthropogenic secondary OA (SOA) precursors during
 14 winter, leading to a different $(C_2H_3O^+ : CO_2^+)_{OOA}$ seasonality in comparison with previous
 15 offline-AMS studies (Daellenbach et al., 2016, Bozzetti et al. 2016a), which were conducted
 16 either at rural sites characterized by different types of vegetation, or in smaller urban areas. In
 17 general, several parameters affect the biogenic SOA concentrations and their separation, e.g.
 18 intensity of the biogenic precursor sources, air masses photochemical age, and NO_x
 19 concentrations. All those parameters were different in Marseille from previous offline-AMS
 20 studies which were conducted in central/northern Europe.

21

22 **4. Results and discussion**

23 **4.1 OA source apportionment results and uncertainties.**

24 In this study, we present one of the first OA source apportionments conducted over an entire
 25 year in the Mediterranean region. This work represents also the first comparison between HR
 26 online-AMS and HR offline-AMS source apportionments conducted at the same location,
 27 despite in two different periods. Previous studies (Daellenbach et al., 2016) reported a
 28 comparison between offline-AMS and online-ACSM results.

29 Although related to different years and size-fractions (PM_{10} online-AMS, $PM_{2.5}$ offline-AMS),
 30 the offline-AMS source apportionment returned average seasonal factor concentrations not

1 statistically different to online-AMS for both winter (Fig. 7) and summer (comparison with El
2 Haddad et al., 2013, Fig. 8). We note that the total OC concentration quantified by online-
3 AMS for PM_1 and by the thermal-optical procedure used for the offline-AMS source
4 apportionment of $PM_{2.5}$ was not different on a seasonal scale considering our uncertainty
5 which includes time variability and measurements uncertainties.

6 Both online and offline-AMS source apportionment revealed that BBOA was the largest OA
7 source during winter. Offline-AMS source apportionment estimated an average BBOA
8 concentration during winter 2011-2012 of $5.2 \mu\text{g m}^{-3}_{\text{avg}}$, representing $43\%_{\text{avg}}$ of the OA.
9 Similarly, online-AMS source apportionment revealed a BBOA concentration of $4.4_{\text{avg}} \mu\text{g m}^{-3}$
10 (corresponding to 42% of OA) during February 2011. During summer, the offline-AMS
11 BBOA concentration dropped to an average of $0.3 \mu\text{g m}^{-3}_{\text{avg}}$ representing 5% of the OA. Not
12 surprisingly such low BBOA contributions were not resolved by online-AMS source
13 apportionment during summer (El Haddad et al., 2013). On average the offline-AMS BBOA
14 relative uncertainty was 9%. As a comparison, the online-AMS BBOA average relative
15 uncertainty was 6%. Overall for both online- and offline-AMS, the BBOA contributions were
16 the least uncertain among the primary sources, possibly because of the high loadings and the
17 distinct seasonal and diurnal BBOA variability in comparison with the other separated factors.
18 A comparison between the offline- and online-AMS source apportionment uncertainties can
19 be carried out with the caveat that the online-AMS source apportionment uncertainties
20 estimated in this work should be considered as a low estimate as they do not account for the
21 AMS mass error deriving mostly from CE, and particle transmission. This source of
22 uncertainty affects the total OA mass but not the relative contribution of the factors. By
23 contrast, the OA mass uncertainty was accounted for in the offline-AMS source
24 apportionment as the OA mass was rescaled to external measurements (WSOC and OC), the
25 uncertainty of which was propagated in the final source apportionment error (Section 2.4).

26 On a yearly scale, the offline-AMS source apportionment revealed that OOA was the largest
27 OA source, with the highest relative contributions during summer due to the reduced BBOA
28 emissions. The OOA concentration during summer was estimated from offline-AMS at $3.0 \mu\text{g m}^{-3}_{\text{avg}}$,
29 corresponding to 55% of the OA mass. El Haddad et al. (2013) also reported OOA to
30 be the dominant OA fraction during summer with a similar average concentration of $2.9 \mu\text{g m}^{-3}$.
31 During winter, the OOA concentration was estimated by online-AMS to be $3.9_{\text{avg}} \mu\text{g m}^{-3}$
32 corresponding to 38% of the OA, while the OOA relative uncertainty was 4%. As a

1 comparison, the OOA relative uncertainty from offline-AMS was 6%_{avg}. The offline-AMS
2 source apportionment revealed similar OOA concentrations during winter (3.4 $\mu\text{g m}^{-3}$ _{avg}
3 corresponding to 27%_{avg} of the OA). Even though during winter the OOA concentration was
4 higher than in summer, possibly due to partitioning and due to the shallower boundary layer,
5 the relative contribution decreased because of the strong BBOA contributions.

6 HOA is one of the most uncertain factors, with an average relative uncertainty of 39%
7 estimated from offline-AMS and 10% from online-AMS analysis, where the larger
8 uncertainty observed for offline-AMS derives mostly from the low R_{HOA} and from the lower
9 time resolution which does not capture the traffic diurnal variability. On average, the HOA
10 concentration predicted by offline-AMS was 1.5 $\mu\text{g m}^{-3}$, corresponding to 17% of the OA.
11 The estimated HOA concentration by online-AMS during February 2011 was 1.6 $\mu\text{g m}^{-3}$ _{avg}
12 (16% of OA). These values are higher than the ones of El Haddad et al. (2013) who estimated
13 a traffic contribution of 0.8 $\mu\text{g m}^{-3}$ _{avg} during July 2008.

14 The COA contributions were only minor (average of 0.3 $\mu\text{g m}^{-3}$), representing on average 4%
15 of the OA mass according to the offline-AMS source apportionment. The online-AMS winter
16 source apportionment returned similar concentrations with 0.4 $\mu\text{g m}^{-3}$ _{avg}, equivalent to 4%_{avg}
17 of the OA. Overall, due to the low concentrations, the COA contributions were uncertain in
18 both source apportionments (6% for online-AMS, 73% for offline-AMS). Similarly to HOA,
19 the larger uncertainty observed for offline-AMS was most possibly due to the low R_{COA} , and
20 the low time resolution which did not enable the COA separation based on the diurnal
21 variability. The summer COA contribution was not resolved from HOA by El Haddad et al.
22 (2013), possibly because the COA reference mass spectrum was not constrained and because
23 of the lack of HR data which typically aid the separation of the two sources.

24 Finally, the INDOA factor concentration estimated from offline-AMS was on average 2.1 μg
25 m^{-3} during winter and 0.6 $\mu\text{g m}^{-3}$ _{avg} during summer, where this seasonal trend was driven by a
26 strong episode that occurred during early February. The offline-AMS relative uncertainty was
27 estimated as 17%. As previously discussed (Section 3.1), this factor was not separated by
28 online-AMS analysis (February 2011) because of the absence of clear events, which in the
29 offline-AMS dataset were observed only over a short period during January-February 2012.
30 An industrial factor was instead resolved by El Haddad et al. (2013) during summer 2008,
31 with an average concentration of 0.3 $\mu\text{g m}^{-3}$ _{avg}. In that study, the industrial OA factor was also
32 characterized by a low background intercepted by ten-fold spiking episodes.

1 From the sum of the offline-AMS factor concentrations we estimated the total OM mass.
2 Using this OM and the measured OC we calculated the OM:OC ratio to be 1.40 on average.
3 Specifically, during winter this ratio was 1.55, which is consistent with the online-AMS
4 values determined from the HR-AMS spectra (median = 1.52, 1st quartile = 1.46; 3rd quartile
5 1.59). The bulk OM:OC variability was driven by the source variabilities. Indeed the relative
6 contribution of the most oxidized source (OOA) was higher during summer (mostly due to the
7 absence of BBOA), however also the relative contributions of the less oxidized sources (such
8 as HOA and COA) were higher during summer mostly due to low BBOA contributions. The
9 BBOA mass spectrum instead was associated with intermediate OM:OC ratios comprised
10 between the values of COA and OOA, and therefore influenced less strongly the bulk OM:OC
11 ratio. Overall the combination of these effects led to a higher bulk OM:OC during winter.

12

13 **4.2 Insights into the BBOA origin during winter**

14 Methyl-nitrocatechols measurements showed high correlations with BBOA (Fig. 9, $R=0.95$)
15 and no correlation with OOA ($R=0.06$, offline-AMS source apportionment). Similarly high
16 correlations were already observed in other studies (e.g. Poulain et al., 2011). This large
17 correlation difference suggests that the variability of the methyl-nitrocatechols is likely
18 explained by the BBOA source. However, methyl-nitrocatechols are secondary compounds
19 deriving from the nitration of catechols which can be either directly emitted by wood
20 combustion (Schauer et al., 2001), or generated by OH· oxidation of cresols directly released
21 by wood combustion (Iinuma et al., 2010). *m*-cresol/NO_x photooxidation experiments (Iinuma
22 et al., 2010) revealed a total contribution of all methyl-nitrocatechol isomers to the catechol
23 SOA of approximately 10%. Assuming methyl-nitrocatechols to be entirely apportioned to the
24 BBOA factor, we estimate a methyl-nitrocatechol-SOA contribution to BBOA on the order of
25 8%, indicating that part of the BBOA factor is of secondary origin. Previous studies (Atkinson
26 and Arey, 2003) revealed an *o*-cresol life-time in the atmosphere of 2.4 minutes towards NO₃,
27 and 3.4 h towards OH (at 298 K, dark conditions). This would suggest that such fast SOA
28 formation can be better traced by the high time resolution online-AMS source apportionment
29 (8 minutes) than by the offline-AMS with 24 h time resolution, and in any case only in the BB
30 plume or in the vicinity of the emission source. Nevertheless we did not observe statistically
31 different ratios (within 1 σ , error calculated as the time variability) of OOA:NH₄⁺ (1.5_{avg} and

1 1.25_{avg} for the offline-AMS and online-AMS source apportionments, respectively),
2 OOA:BBOA (0.65_{avg} and 0.89_{avg} respectively), and levoglucosan:BBOC (1.13_{avg} and 1.15_{avg}
3 respectively, Fig. 10) during winter, suggesting that despite the different time resolutions, the
4 online and offline methods provide a comparable BBOA-SOA separation. Overall these
5 findings suggest that rapid SOA formation is not well captured by PMF and rapidly formed
6 SOA compounds (such as nitrocatechols) can be systematically attributed by PMF to factors
7 commonly considered as “primary” (BBOA in this case). Both online- and offline-AMS
8 source apportionment revealed for the two different winter seasons a comparable temporal
9 evolution of the levoglucosan:BBOC ratio (Fig. 10, and Fig. 11). This ratio showed typical
10 literature values for domestic wood combustion in Europe during January and early February
11 (0.05-0.2, Zotter et al., 2014; Herich et al., 2014; Minguillón et al., 2011), while during late
12 autumn and March (Fig. 11) it increased up to 0.3, highlighting an evolution of the BBOA
13 chemical composition. A similar seasonal trend was observed for the levoglucosan:vanillic
14 acid, levoglucosan:syringic acid, and levoglucosan:non sea salt-K⁺ (nss-K⁺, calculated
15 according to Seinfeld and Pandis, 2006) ratios (Fig. 11). Although the online dataset was
16 limited to one month of measurements, the levoglucosan:vanillic acid ratio also showed a
17 statistically significant increasing trend from early February to the beginning of March
18 (confidence interval of 95%, Mann-Kendall test). These results suggest the occurrence of
19 different types of biomass combustions during low temperature winter days compared to late
20 autumn and early spring: as levoglucosan derives from cellulose pyrolysis (>300°C), while
21 vanillic and syringic acid result from lignin combustion (Simoneit et al., 1998, Sullivan et al.,
22 2008). Different reactivities / volatilities of BBOA markers may complicate this analysis. For
23 this reason we discuss in the following the levoglucosan stability, and propose that the major
24 driver of the observed seasonal trends is the occurrence of different BBOA combustions.

25 Previous studies revealed the levoglucosan reactivity toward OH· radical oxidation (Hennigan
26 et al., 2010) both in gas and aqueous phase (Hoffmann et al., 2010). In the following we
27 analyze the levoglucosan and nss-K⁺ time series in order to investigate the possible effects of
28 levoglucosan chemical stability and different types of biomass combustions on the seasonal
29 evolution of the levoglucosan:nss-K⁺ ratio. During summer nss-K⁺ derives mostly from dust,
30 while levoglucosan is depleted by both photochemistry (Hennigan et al., 2010) and low
31 BBOA emissions. Not surprisingly the levoglucosan:nss-K⁺ ratio showed lower average
32 values in summer (0.23) than in winter (3.14). During winter nss-K⁺ is considered to be
33 mostly emitted by BBOA, and consistently in our dataset it shows a good correlation with

1 BBOA tracers ($R=0.66$ with syringic acid). Overall, the levoglucosan:nss- K^+ ratio during the
2 cold season manifests a behavior that is opposite to the photochemical activity (with
3 temperature considered as a proxy) as it shows higher values during March and late autumn
4 (up to 7.11) and lower in January, February (minimum = 2.79; Fig. 11) when temperature is
5 lower and photochemistry is less intense. For these reasons we relate the winter
6 levoglucosan:nss- K^+ variability to different types of combustion rather than to a levoglucosan
7 depletion due to photochemistry. Furthermore we observed the highest levoglucosan
8 concentrations (late autumn) simultaneously with the highest relative humidity (89%) values,
9 suggesting the depletion of levoglucosan by $OH\cdot$ radical oxidation in aqueous phase to be not
10 significant (Hoffmann et al., 2010).

11 A similar winter seasonal behavior was observed also for plant waxes. Plant waxes
12 concentrations were estimated from high molecular weight *n*-alkanes (C24-C35) according to
13 the methodology described by Li et al. (2010). This methodology is based on the observation
14 that alkanes from epicuticular waxes preferentially contain an odd number of carbon atoms
15 (Aceves and Grimalt, 1993; Simoneit et al., 1991). This was observed for a large variety of
16 plants including broad leaf trees, conifers, palms, shrubs, grasses, and groundcover
17 (Hildemann et al., 1996 and references therein). Waxes showed the highest concentrations
18 during late autumn (up to $0.16 \mu\text{g m}^{-3}$) and in May (up to $0.17 \mu\text{g m}^{-3}$), while the minima were
19 observed during winter (minimum $0.007 \mu\text{g m}^{-3}$). In general, high molecular weight *n*-alkanes
20 are typically detected in atmospheric aerosol in significant amounts during the growing
21 season. In a similar way, Hildemann et al. (1996) estimated the highest plant waxes
22 concentrations in April-May in Los Angeles and Pasadena where the climate is similar to
23 Marseille. Similarly we observed the highest concentrations during May. However,
24 comparable plant waxes concentrations were observed also in late autumn during the period
25 characterized by the highest levoglucosan:lignin combustion tracers (Fig 11), suggesting a
26 possible emission from open combustion of green wastes.

27 Taken together the above observations suggest the occurrence of combustion of cellulose-rich
28 material during March and late autumn, compared to lignin rich biomass burning for
29 residential heating during January. The combustion of cellulose-rich material is possibly
30 related to agricultural waste burning at the beginning and at the end of the agricultural cycle.
31 The occurrence of emission of biomass plumes due to land clearing episodes during March
32 has already been reported in other parts of Europe (Ulevicius et al., 2016), and has been

1 previously modelled for southern France (Dernier van der Gon et al., 2015, Fountoukis et al.,
2 2014).

3 In this study we related the evolution of the BB composition over the cold season to the
4 combustion of cellulose-rich and lignin-rich fuels, considering that lignin and cellulose are
5 contained in different ratios in different biomass fuels. This designation should not be
6 considered as an oversimplification of the combustion processes or of the fuel complexity, but
7 rather as a classification of the BB aerosol based on our observations of increasing lignin
8 pyrolysis products over cellulose pyrolysis products during the coldest days.

9 We note that BB is described in our PMF models by only one factor which therefore
10 potentially represents a combination of several types of biomass burning sources. Increasing
11 the number of factors did not lead to an unambiguous separation of different BBOA sources,
12 however, the comparison with source-specific markers revealed a real BBOA composition
13 evolution over the winter season with higher cellulose to lignin combustion tracer ratios
14 observed during late autumn and early spring in comparison to January/February. This
15 hypothesis of at least two types of BB sources (one linked to domestic heating, another to
16 agricultural activities) is also supported by the direct PMF analysis of the organic and
17 inorganic markers measured for batch 1 (Salameh et al., *submitted*).

18

19 **5 Conclusions**

20 PM_{2.5} filter samples were collected during an entire year (August 2011 to July 2012) at an
21 urban site in Marseille, France. Filter samples were analyzed by water extraction followed by
22 nebulization of the liquid extracts and subsequent measurement of the generated aerosol with
23 an HR-ToF-AMS (Daellenbach et al., 2016).

24 PMF analysis was conducted on the offline-AMS mass spectra and on online-AMS data
25 collected at the same station during February 2011. Offline-AMS source apportionment
26 results were also compared with a previous online-AMS source apportionment study of two
27 weeks during July 2008 at the same location (El Haddad et al., 2013). The methods returned
28 statistically similar seasonal factor concentrations, although different years and size fractions
29 were considered (PM₁ for online-AMS, PM_{2.5} for offline-AMS). OOA was the major source
30 of OA during summer representing on average 55% of the OA mass, while BBOA was the
31 dominant OA source during winter contributing on average 43% of the OA. Smaller

1 contributions were estimated for HOA, INDOA and COA, representing 17%, 12%, and 4% of
2 the OA mass, respectively. The contribution of primary anthropogenic sources (HOA +
3 BBOA + COA + INDOA) was substantial over the year (62%_{avg} of OA), with larger absolute
4 and relative contributions during winter (73% of OA_{avg}) associated with an intense biomass
5 burning activity.

6 Coupling offline- and online-AMS data with molecular markers showed increasing
7 levoglucosan:BBOC ratios during the late winter-early spring period in both 2011 and 2012.
8 This trend was also observed for the ratios between cellulose and lignin combustion markers
9 (e.g. levoglucosan:vanillic acid), with ratios approaching more typical domestic wood
10 combustion European values during January/early February, and values characterized by
11 higher values of cellulose-combustion markers during late autumn and March indicative of
12 the influence of different types of fuels, possibly related to agricultural-related activities.

13 From the offline-AMS source apportionment, we observed a high BBOA correlation with
14 nitrocatechols deriving from the nitration of catechols directly emitted by biomass
15 combustion. These secondary components are rapidly formed in the atmosphere in presence
16 of NO₃[·] (life time of a few minutes). Overall, despite the different time resolution, online- and
17 offline-AMS provided a comparable SOA-BBOA separation during winter. Nevertheless, in
18 case of fast SOA formation (relative to the time scale of the online-AMS time resolution, or
19 relative to the transport time to the receptor site) this separation can be hindered, and further
20 efforts are needed to improve the SOA separation from BBOA.

21

22 **Authors contributions:**

23 Experimental design: A. S. H. Prévôt, I. El Haddad, N. Marchand, and C. Bozzetti

24 Filter collections and online-AMS measurements: N. Marchand and D. Salameh.

25 Offline-AMS analysis: C. Bozzetti, E. Müller, K. R. Daellenbach, and I. El Haddad

26 WSOC and TN analysis: P. Fermo and R. Gonzalez

27 Sunset, and IC analysis: J.-L. Jaffrezo

28 GC-MS analysis: D. Salameh, and N. Marchand

29 Nitrocatechols analysis: Y. Iinuma

- 1 Carbonates analysis: M. C. Minguillón
- 2 Data analysis and validation: C Bozzetti, and I. El Haddad
- 3 PMF analysis: C. Bozzetti
- 4 All authors read and commented on the manuscript.

5

6 **Acknowledgements**

7 CB thanks the Lithuanian–Swiss Cooperation Programme “Research and Development”
8 project AEROLIT (Nr. CH-3-MM-01/08). JGS acknowledges the support of the Swiss
9 National Science Foundation (Starting Grant No. BSSGI0 155846). IE-H acknowledges the
10 support of the Swiss National Science Foundation (IZERZO 142146). This work has also been
11 supported by the MED program (APICE, grant number 2G-MED09-026: [http://www.apice-](http://www.apice-project.eu/)
12 [project.eu/](http://www.apice-project.eu/)), the French Environment and Energy Management Agency (ADEME) and
13 Provence Alpes Cote d'Azur Region (PACA). Part of the OC/EC analysis carried out in MRS
14 has been supported by the French national CARA program. This program is directed by O.
15 Favez (INERIS; <http://www.ineris.fr/>). He is gratefully acknowledged.

16

1 **References**

2

3 Aceves, M. and Grimalt, J. O.: Seasonally dependent size distributions of aliphatic and
4 polycyclic aromatic hydrocarbons in urban aerosols from densely populated areas, *Environ.*
5 *Sci. Technol.*, 27(13), 2896–2908, doi:10.1021/es00049a033, 1993.

6 Aiken, A. C., DeCarlo, P. F., Kroll, J. H., Worsnop, D. R., Huffman, J. A., Docherty, K. S.,
7 Ulbrich, I. M., Mohr, C., Kimmel, J. R., Sueper, D., Sun, Y., Zhang, Q., Trimborn, A.,
8 Northway, M., Ziemann, P. J., Canagaratna, M. R., Onasch, T. B., Alfarra, M. R., Prevot, A.
9 S. H., Dommen, J., Duplissy, J., Metzger, A., Baltensperger, U., and Jimenez J. L. O/C and
10 OM:OC ratios of primary, secondary, and ambient organic aerosols with high-resolution time-
11 of-flight aerosol mass spectrometry. *Environ. Sci. Technol.* 42, 4478-4485, 2008.

12 Aksoyoglu, S., Keller, J., Barmpadimos, I., Oderbolz, D., Lanz, V. A., Prévôt, A. S. H., and
13 Baltensperger U.: Aerosol modelling in Europe with a focus on Switzerland during summer
14 and winter episodes, *Atmos. Chem. Phys.*, 11, 7355–7373, 2011.

15 Aksoyoglu, S., Keller, J., Ciarelli, G., Prévôt, A. S. H., and Baltensperger, U.: A model study
16 on changes of European and Swiss particulate matter, ozone and nitrogen deposition between
17 1990 and 2020 due to the revised Gothenburg protocol, *Atmos. Chem. Phys.*, 14, 13081-
18 13095, doi:10.5194/acp-14-13081-2014, 2014.

19 Alfarra, M. R., Prévôt, A. S. H., Szidat, S., Sandradewi, J., Weimer, S., Lanz, V. A.,
20 Schreiber, D., Mohr, M., and Baltensperger, U.: Identification of the mass spectral signature
21 of organic aerosols from wood burning emissions, *Environ. Sci. Technol.*, 41, 5770–5777,
22 2007.

23 Allan, J. D., Jimenez, J. L., Williams, P. I., Alfarra, M. R., Bower, K. N., Jayne, J. T., Coe,
24 H., and Worsnop, D. R.: Quantitative sampling using an Aerodyne aerosol mass spectrometer:
25 1. Techniques of data interpretation and error analysis, *J. Geophys. Res.-Atmos.*, 108, 4090,
26 2003.

27 Atkinson, R., and Arey, J.: Atmospheric degradation of volatile organic compounds, *Chem.*
28 *Rev.*, 103, 4605-4638, 2003.

29 Baklanov, A., Schlünzen, K., Suppan, P., Baldasano, J., Brunner, D., Aksoyoglu, S.,
30 Carmichael, G., Douros, J., Flemming, J., Forkel, R., Galmarini, S., Gauss, M., Grell, G.,

1 Hirtl, M., Joffre, S., Jorba, O., Kaas, E., Kaasik, M., Kallos, G., Kong, X., Korsholm, U.,
2 Kurganskiy, A., Kushta, J., Lohmann, U., Mahura, A., Manders-Groot, A., Maurizi, A.,
3 Moussiopoulos, N., Rao, S. T., Savage, N., Seigneur, C., Sokhi, R. S., Solazzo, E.,
4 Solomos, S., Sørensen, B., Tsegas, G., Vignati, E., Vogel, B., and Zhang, Y.: Online coupled
5 regional meteorology chemistry models in Europe: current status and prospects, *Atmos.*
6 *Chem. Phys.*, 14, 317-398, doi:10.5194/acp-14-317-2014, 2014.

7 Birch, M. E. and Cary, R. A.: Elemental carbon-based method for monitoring occupational
8 exposures to particulate diesel exhaust, *Aerosol Sci. and Tech.*, 25, 221–241, 1996.

9 Bozzetti, C., Daellenbach, K., R., Hueglin, C., Fermo, P., Sciare, J., Kasper-Giebl, A., Mazar,
10 Y., Abbaszade, G., El Kazzi, M., Gonzalez, R., Shuster Meiseles, T., Flasch, M., Wolf, R.,
11 Křepelová, A., Canonaco, F., Schnelle-Kreis, J., Slowik, J. G., Zimmermann, R., Rudich, Y.,
12 Baltensperger, U., El Haddad, I., and Prévôt, A. S. H.: Size-resolved identification,
13 characterization, and quantification of primary biological organic aerosol at a European rural
14 site, *Environ. Sci. Technol.*, 50, 3425-3434, doi:10.1021/acs.est.5b05960, 2016.

15 Bozzetti, C., Sosedova, Y., Xiao, M., Daellenbach, K. R., Ulevicius, V., Dudoitis, V.,
16 Mordas, G., Byčenkienė, S., Plauškaitė, K., Vlachou, A., Golly, B., Chazneau, B., Besombes,
17 J.-L., Baltensperger, U., Jaffrezo, J.-L., Slowik, J. G., El Haddad, I., and Prévôt, A. S. H.:
18 Argon offline-AMS source apportionment of organic aerosol over yearly cycles for an urban,
19 rural and marine site in Northern Europe, *Atmos. Chem. Phys.* 17, 117–141, 2017.

20 Brown, S. G., Eberly, S., Paatero, P., and Norris, G. A., Methods for estimating uncertainty in
21 PMF solutions: Examples with ambient air and water quality data and guidance on reporting
22 PMF results, *Sci. Tot. Environ.* 518-519, 626-635, 2015.

23 Bruns, E. A., Krapf, M., Orasche, J., Huang, Y., Zimmermann, R., Drinovec, L., Močnik, G.,
24 El-Haddad, I., Slowik, J. G., Dommen, J., Baltensperger, U. and Prévôt, A. S. H.:
25 Characterization of primary and secondary wood combustion products generated under
26 different burner loads, *Atmos. Chem. Phys.*, 15, 2825–2841, 2015.

27 Canagaratna, M. R., Jayne, J. T., Jimenez, J. L., Allan, J. D., Alfarra, M. R., Zhang, Q.,
28 Onasch, T. B., Drewnick, F., Coe, H., Middlebrook, A., Delia, A., Williams, L. R., Trimborn,
29 A. M., Northway, M. J., DeCarlo, P. F., Kolb, C. E., Davidovits, P. and Worsnop, D. R.:
30 Chemical and microphysical characterization of ambient aerosols with the Aerodyne aerosol
31 mass spectrometer, *Mass Spectrom. Rev.* 26:185-222, 2007.

1 Canonaco, F., Crippa, M., Slowik, J. G., Baltensperger, U., and Prévôt, A. S. H.: SoFi, an
2 IGOR-based interface for the efficient use of the generalized multilinear engine (ME-2) for
3 the source apportionment: ME-2 application to aerosol mass spectrometer data, *Atmos. Meas.*
4 *Tech.*, 6, 3649-3661, 2013.

5 Canonaco, F., Slowik, J. G., Baltensperger, U., and Prévôt, A. S. H.: Seasonal differences in
6 oxygenated organic aerosol composition: implications for emissions sources and factor
7 analysis. *Atmos. Chem. Phys.* 15, 6993-7002, 2015.

8 Cavalli, F., Viana, M., Yttri, K. E., Genberg, J., and Putaud, J. P.: Toward a standardised
9 thermal-optical protocol for measuring atmospheric organic and elemental carbon: the
10 EUSAAR protocol, *Atmos. Meas. Tech.*, 3, 79-89, 2010.

11 Chauvel, C., Bureau, S., and Poggi, C.: Comprehensive chemical and isotopic analyses of
12 basalt and sediment reference materials, *Geostand. Geoanalyt. Res.*, 35, 125–143, doi:
13 10.1111/j.1751-908X.2010.00086.x, 2010.

14 Crippa, M., Canonaco, F., Slowik, J. G., El Haddad, I., DeCarlo, P. F., Mohr, C., Heringa, M.
15 F., Chirico, R., Marchand, N., Temime-Roussel, B., Abidi, E., Poulain, L., Wiedensohler, A.,
16 Baltensperger, U., and Prévôt, A. S. H.: Primary and secondary organic aerosol origin by
17 combined gas-particle phase source apportionment, *Atmos. Chem. Phys.*, 13, 8411-8426,
18 doi:10.5194/acp-13-8411-2013, 2013a.

19 Crippa, M., El Haddad, I., Slowik, J. G., DeCarlo, P.F., Mohr, C., Heringa, M. F., Chirico, R.,
20 Marchand, N., L., Sciare, J., Baltensperger, U., and Prévôt, A. S. H.: Identification of marine
21 and continental aerosol sources in Paris using high resolution aerosol mass spectrometry, *J.*
22 *Geophys. Res.*, 118, 1950-1963, 2013b.

23 Daellenbach, K. R., Bozzetti, C., Krepelova, A., Canonaco, F., Huang, R.-J., Wolf, R., Zotter,
24 P., Crippa, M., Slowik, J., Zhang, Y., Szidat, S., Baltensperger, U., Prévôt, A. S. H., and El
25 Haddad, I.: Characterization and source apportionment of organic aerosol using offline
26 aerosol mass spectrometry, *Atmos. Meas. Tech.*, 9, 23-39, 2016.

27 Davison, A. C. and Hinkley, D. V.: *Bootstrap Methods and Their Application*, Cambridge
28 University Press, Cambridge, UK, 582 pp., 1997.

29 DeCarlo, P. F., Kimmel, J. R., Trimborn, A., Northway, M. J., Jayne, J. T., Aiken, A. C.,
30 Gonin, M., Fuhrer, K., Horvath, T., Docherty, K. S., Worsnop, D. R., and Jimenez, J. L.:

1 Field-deployable, high-resolution, time-of-flight aerosol mass spectrometer, *Anal. Chem.*, 78,
2 8281–8289, 2006.

3 Denier van der Gon, H. A. C., Bergström, R., Fountoukis, C., Johansson, C., Pandis, S. N.,
4 Simpson, D., and Visschedijk, A. J. H.: Particulate emissions from residential wood
5 combustion in Europe – revised estimates and an evaluation, *Atmos. Chem. Phys.*, 15, 6503-
6 6519, doi:10.5194/acp-15-6503-2015, 2015.

7 Docherty, K. S., Aiken, A. C., Huffman, J. A., Ulbrich, I. M., DeCarlo, P. F., Sueper,
8 D., Worsnop, D. R., Snyder, D. C., Peltier, R. E., Weber, R. J., Grover, B. D., Eatough, D. J.,
9 Williams, B. J., Goldstein, A. H., Ziemann, P. J., and Jimenez, J. L.: The 2005 Study of
10 organic aerosols at riverside (SOAR-1): instrumental intercomparisons and fine particle
11 composition, *Atmos. Chem. Phys.*, 11, 12387-12420, 2011.

12 Dockery, D. W., Luttmann-Gibson, H., Rich, D. Q., Link, M. S., Mittleman, M. A., Gold, D.
13 R., Koutrakis, P., Schwartz, J. D., and Verrier, R. L.: Association of air pollution with
14 increased incidence of ventricular tachyarrhythmias recorded by implanted cardioverter
15 defibrillators, *Environ. Health Perspect.* 113, 670-674, 2005.

16 Drewnick, F., Hings, S. S., DeCarlo, P. F., Jayne, J. T., Gonin, M., Fuhrer, K., Weimer, S.,
17 Jimenez, J. L., Demerjian, K. L., Borrmann, S., and Worsnop, D. R.: A new time-of-flight
18 aerosol mass spectrometer (ToF-AMS) – instrument description and first field deployment,
19 *Aerosol Sci. Tech.*, 39, 637–658, 2005.

20 Drobinski, P., Said, F., Arteta, J., Augustin, P., Bastin, S., Brut, A., Caccia, J. L., Campistron,
21 B., Cautenet, S., Colette, A., Coll, I., Corsmeier, U., Cros, B., Dabas, A., Delbarre, H.,
22 Dufour, A., Durand, P., Guenard, V., Hasel, M., Kalthoff, N., Kottmeier, C., Lasry, F.,
23 Lemonsu, A., Lohou, F., Masson, V., Menut, L., Moppert, C., Peuch, V. H., Puygrenier, V.,
24 Reitebuch, O., and Vautard, R.: Regional transport and dilution during high-pollution
25 episodes in southern France: Summary of findings from the Field Experiment to Constraint
26 Models of Atmospheric Pollution and Emissions Transport (ESCOMPTE), *J. Geophys. Res.-*
27 *Atmos.*, 112, D13105, doi:10.1029/2006JD007494, 2007.

28 Dzepina, K., Arey, J., Marr, L.C., Worsnop, D.R., Salcedo, D., Zhang, Q., Onasch, T.B.,
29 Molina L.T., Molina M. J., Jimenez, J.L.: Detection of particle-phase polycyclic aromatic
30 hydrocarbons in Mexico City using an aerosol mass spectrometer, *International Journal of*
31 *Mass Spectrometry*, 263, 152–170, 2007.

1 El Haddad, I., D'Anna, B., Temime-Roussel, B., Nicolas, M., Boreave, A., Favez, O., Voisin,
2 D., Sciare, J., George, C., Jaffrezo, J.-L., Wortham, H., and Marchand, N.: Towards a better
3 understanding of the origins, chemical composition and aging of oxygenated organic aerosols:
4 case study of a Mediterranean industrialized environment, Marseille, *Atmos. Chem. Phys.*, 13,
5 7875–7894, 2013.

6 El Haddad, I., Marchand, N., Dron, J., Temime-Roussel, B., Quivet, E., Wortham, H.,
7 Jaffrezo, J. L., Baduel, C., Voisin, D., Besombes, J. L., and Gille, G.: Comprehensive primary
8 particulate organic characterization of vehicular exhaust emissions in France, *Atmos.*
9 *Environ.*, 43, 6190–6198, 2009.

10 El Haddad, I., Marchand, N., Wortham, H., Piot, C., Besombes, J.-L. , Cozic, J., Chauvel,
11 C., Armengaud, A., Robin D., and Jaffrezo, J.-L.: Primary sources of PM_{2.5} organic aerosol in
12 an industrial Mediterranean city, Marseille, *Atmos. Chem. Phys.*, 11, 2039-2058, 2011.

13 Elser, M., Huang, R.-J., Wolf, R., Slowik, J. G., Wang, Q., Canonaco, F., Li, G., Bozzetti, C.,
14 Daellenbach, K. R., Huang, Y., Zhang, R., Li, Z., Cao, J., Baltensperger, U., El-Haddad, I.,
15 and Prévôt, A. S. H.: New insights into PM_{2.5} chemical composition and sources in two
16 major cities in China during extreme haze events using aerosol mass spectrometry, *Atmos.*
17 *Chem. Phys.*, 16, 3207-3225, doi:10.5194/acp-16-3207-2016, 2016.

18 Favez, O., El Haddad, I., Piot, C., Boréave, A., Abidi, E., Marchand, N., Jaffrezo, J.-L.,
19 Besombes, J.-L., Personnaz, M.-B., Sciare, J., Wortham, H., George, C., and D'Anna, B.:
20 Inter-comparison of source apportionment models for the estimation of wood burning
21 aerosols during wintertime in an Alpine city (Grenoble, France), *Atmos. Chem. Phys.*, 10,
22 5295–5314, doi:10.5194/acp-10-5295- 2010, 2010.

23 Flaounas, E., Coll, I., Armengaud, A., and Schmechtig, C.: The representation of dust
24 transport and missing urban sources as major issues for the simulation of PM episodes in a
25 Mediterranean area, *Atmos. Chem. Phys.*, 9, 8091–8101, doi:10.5194/acp-9-80912009, 2009.

26 Fountoukis, C., Megaritis, A. G., Skyllakou, K., Charalampidis, P. E., Pilinis, C., Denier van
27 der Gon, H. A. C., Crippa, M., Canonaco, F., Mohr, C., Prévôt, A. S. H., Allan, J. D., Poulain,
28 L., Petäjä, T., Tiitta, P., Carbone, S., Kiendler-Scharr, A., Nemitz, E., O'Dowd, C., Swietlicki,
29 E., and Pandis, S. N.: Organic aerosol concentration and composition over Europe: insights
30 from comparison of regional model predictions with aerosol mass spectrometer factor
31 analysis, *Atmos. Chem. Phys.*, 14, 9061-9076, doi:10.5194/acp-14-9061-2014, 2014.

- 1 Garcia, E.: A Tutorial on Correlation Coefficients, [http://web.simmons.edu/~benoit/lis642/a-](http://web.simmons.edu/~benoit/lis642/a-tutorial-on-correlation-coefficients.pdf)
2 [tutorial-on-correlation-coefficients.pdf](http://web.simmons.edu/~benoit/lis642/a-tutorial-on-correlation-coefficients.pdf), pp. 7-8, 2011.
- 3 He, L.-Y., Lin, Y., Huang, X.-F., Guo, S., Xue, L., Su, Q., Hu, M., Luan, S.-J., and Zhang,
4 Y.-H.: Characterization of high-resolution aerosol mass spectra of primary organic aerosol
5 emissions from Chinese cooking and biomass burning, *Atmos. Chem. Phys.*, 10, 11535-
6 11543, doi:10.5194/acp-10-11535-2010, 2010.
- 7 Hennigan, C. J., Sullivan, A. P., Collett, J. L., and Robinson, A. L.: Levoglucosan stability in
8 biomass burning particles exposed to hydroxyl radicals, *Geophys. Res. Lett.*, 37, L09806,
9 doi:10.1029/2010GL043088, 2010.
- 10 Herich, H., Gianini, M. F. D., Piot, C., Mocnik, G., Jaffrezo, J. L., Besombes, J. L., Prévôt, A.
11 S. H., and Hueglin, C.: Overview of the impact of wood burning emissions on carbonaceous
12 aerosols and PM in large parts of the Alpine region, *Atmos. Environ.*, 89, 64–75,
13 doi:10.1016/j.atmosenv.2014.02.008, 2014.
- 14 Hildebrandt, L., Kostenidou, E., Lanz, V. A., Prevot, A. S. H., Baltensperger, U.,
15 Mihalopoulos, N., Laaksonen, A., Donahue, N. M., and Pandis, S. N.: Sources and
16 atmospheric processing of organic aerosol in the Mediterranean: insights from aerosol mass
17 spectrometer factor analysis, *Atmos. Chem. Phys.*, 11, 12499-12515, doi:10.5194/acp-11-
18 12499-2011, 2011.
- 19 Hildebrandt, L., Kostenidou, E., Mihalopoulos, N., Worsnop, D. R., Donahue, N. M., and
20 Pandis, S. N.: Formation of highly oxygen-ated organic aerosol in the atmosphere: Insights
21 from the Finokalia Aerosol Measurement Experiments, *Geophys. Res. Lett.*, 37, L23801,
22 doi:10.1029/2010GL 045193, 2010.
- 23 Huang, R.-J., Zhang, Y., Bozzetti, C., Ho, K.-F., Cao, J., Han, Y., Daellenbach, K. R., Slowik,
24 J. G., Platt, S. M., Canonaco, F., Zotter, P., Wolf, R., Pieber, S. M., Bruns, E. A., Crippa, M.,
25 Ciarelli, G., Piazzalunga, A., Schwikowski, M., Abbaszade, G., Schnelle-Kreis, J.,
26 Zimmermann, R., An, Z., Szidat, S., Baltensperger, U., Haddad, I. E., and Prévôt, A. S. H.:
27 High secondary aerosol contribution to particulate pollution during haze events in China,
28 *Nature*, 514, 218-222, 2014.
- 29 Hildemann, L. M., Rogge, W. F., Cass, G. R., Mazurek, M. A., and Simoneit, B. R. T.:
30 Contribution of primary aerosol emissions from vegetation-derived sources to fine particle

1 concentrations in Los Angeles. *J. Geophys. Res.*, 101, 19,541-19,549, doi:
2 10.1029/95JD02136, 2016.

3 Hoffmann, D., Tilgner A., Iinuma, Y., and Herrmann, H.: Atmospheric stability of
4 levoglucosan: a detailed laboratory and modeling study, *Environ. Sci. Technol.*, 44, 694–699,
5 2010.

6 Iinuma, Y., Böge, O., Gräfe, R., and Herrmann, H.: Methyl-nitrocatechols: Atmospheric
7 tracer compounds or biomass burning secondary organic aerosols, *Environ. Sci. Technol.*, 44,
8 8453–8459, 2010.

9 Jaffrezo, J. L., Calas, T., and Bouchet, M.: Carboxylic acids measurements with ionic
10 chromatography, *Atmos. Environ.*, 32, 2705–2708, 1998.

11 Jayne, J. T., Leard, D. C., Zhang, X. F., Davidovits, P., Smith, K. A., Kolb, C. E., and
12 Worsnop, D. R. (2000). Development of an aerosol mass spectrometer for size and
13 composition analysis of submicron particles, *Aerosol Sci. Technol.* 33, 49–70, 2000.

14 Jimenez, J. L., Canagaratna, M. R., Donahue, N. M., Prevot, A. S. H., Zhang, Q., Kroll, J. H.,
15 DeCarlo, P. F., Allan, J. D., Coe, H., Ng, N. L., Aiken, A. C., Docherty, K. S., Ulbrich, I. M.,
16 Grieshop, A. P., Robinson, A. L., Duplissy, J., Smith, J. D., Wilson, K. R., Lanz, V. A.,
17 Hueglin, C., Sun, Y. L., Tian, J., Laaksonen, A., Raatikainen, T., Rautiainen, J., Vaattovaara,
18 P., Ehn, M., Kulmala, M., Tomlinson, J. M., Collins, D. R., Cubison, M. J., Dunlea, E. J.,
19 Huffman, J. A., Onasch, T. B., Alfarra, M. R., Williams, P. I., Bower, K., Kondo, Y.,
20 Schneider, J., Drewnick, F., Borrmann, S., Weimer, S., Demerjian, K., Salcedo, D., Cottrell,
21 L., Griffin, R., Takami, A., Miyoshi, T., Hatakeyama, S., Shimono, A., Sun, J. Y., Zhang, Y.
22 M., Dzepina, K., Kimmel, J. R., Sueper, D., Jayne, J. T., Herndon, S. C., Trimborn, A. M.,
23 Williams, L. R., Wood, E. C., Middlebrook, A. M., Kolb, C. E., Baltensperger, U., and
24 Worsnop, D. R.: Evolution of organic aerosols in the atmosphere, *Science*, 326, 1525–1529,
25 2009.

26 Karanasiou, A., Diapouli, E., Cavalli, F., Eleftheriadis, K., Viana, M., Alastuey, A., Querol,
27 X., and Reche, C.: On the quantification of atmospheric carbonate carbon by thermal/optical
28 analysis protocols, *Atmos. Meas. Tech.*, 4, 2409–2419, 2011

29 Laden, F., Neas, L. M., Dockery, D. W., and Schwartz, J.: Association of fine particulate
30 matter from different sources with daily mortality in six US cities, *Environ. Health Perspect.*
31 108:941-947, 2000.

1 Lanz, V. A., Alfarra, M. R., Baltensperger, U., Buchmann, B., Hueglin, C., and Prevot, A. S.
2 H.. Source apportionment of submicron organic aerosols at an urban site by factor analytical
3 modelling of aerosol mass spectra, *Atmos. Chem. Phys.* 7:1503-1522, 2007.

4 Lanz, V. A., M. R. Alfarra, U. Baltensperger, B. Buchmann, C. Hueglin, S. Szidat, M. N.
5 Wehrli, L. Wacker, S. Weimer, A. Caseiro, H. Puxbaum, and A. S. H. Prevot: Source
6 attribution of submicron organic aerosols during wintertime inversions by advanced factor
7 analysis of aerosol mass spectra, *Envir. Sci. Tech.*, 42, 214-220, 2008.

8 Lee, A. K. Y., Herckes, P., Leitch, W. R., Macdonald, A. M., and Abbatt, J. P. D.: Aqueous
9 OH oxidation of ambient organic aerosol and cloud water organics: Formation of highly
10 oxidized products, *Geoph. Res. Lett.*, 38, L11 805, doi: 10.1029/2011GL047439, 2011.

11 Li, W., Peng, Y., and Bai, Z.: Distributions and sources of *n*-alkanes in PM_{2.5} at urban,
12 industrial and coastal sites in Tianjin, China, *J. Environ. Sci.*, 22, 1551-1557, 2010.

13 Lohmann, U., Broekhuizen, K., Leitch, R., Shantz, N., and Abbatt, J.: How efficient is cloud
14 droplet formation of organic aerosols?, *Geophys. Res. Lett.* 31, L05108, doi:
15 10.1029/2003GL018999, 2004.

16 Middlebrook, A.M., Bahrein, R., Jimenez, J.L., and Canagaratna, M.R.: Evaluation of
17 composition-dependent collection efficiencies for the Aerodyne aerosol mass spectrometer
18 using field data, *Aerosol Sci. and Tech.*, 46, 258-271, 2012.

19 Mihara, T. and Mochida, M.: Characterization of solvent-extractable organics in urban
20 aerosols based on mass spectrum analysis and hygroscopic growth measurement, *Environ.*
21 *Sci. Technol.*, 45, 9168–9174, 2011.

22 Minguillón M. C., Pérez N., Marchand N., Bertrand A., Temime-Roussel B., Agrios K.,
23 Szidat S., van Drooge B., Sylvestre S., Alastuey A., Reche C., Ripoll A., Marco E., Grimalt J.
24 O., and Querol X.. Secondary organic aerosol origin in an urban environment: influence of
25 biogenic and fuel combustion precursors. *Faraday Discussions*, 189, 337-359, 2016.

26 Minguillón, M. C., Perron, N., Querol, X., Szidat, S., Fahrni, S. M., Alastuey, A., Jimenez, J.
27 L., Mohr, C., Ortega, A. M., Day, D. A., Lanz, V. A., Wacker, L., Reche, C., Cusack, M.,
28 Amato, F., Kiss, G., Hoffer, A., Decesari, S., Moretti, F., Hillamo, R., Teinila, K., Seco, R.,
29 Penuelas, J., Metzger, A., Schallhart, S., Muller, M., Hansel, A., Burkhardt, J. F.,
30 Baltensperger, U., and Prevot, A. S. H.: Fossil versus contemporary sources of fine elemental

1 and organic carbonaceous particulate matter during the DAURE campaign in Northeast Spain,
2 *Atmos. Chem. Phys.*, 11, 12067-12084, 2011.

3 Minguillón, M. C., Ripoll, A., Pérez, N., Prévôt, A. S. H., Canonaco, F., Querol, X., and
4 Alastuey, A.: Chemical characterization of submicron regional background aerosols in the
5 western Mediterranean using an Aerosol Chemical Speciation Monitor, *Atmos. Chem. Phys.*,
6 15, 6379-6391, 2015.

7 Mohr, C., DeCarlo, P. F., Heringa, M. F., Chirico, R., Slowik, J. G., Richter, R., Reche, C.,
8 Alastuey, A., Querol, X., Seco, R., Penuelas, J., Jimenez, J. L., Crippa, M., Zimmermann, R.,
9 Baltensperger, U., and Prevot, A. S. H.: Identification and quantification of organic aerosol
10 from cooking and other sources in Barcelona using aerosol mass spectrometer data, *Atmos.*
11 *Chem. Phys.*, 12, 1649-1665, 2012.

12 Mohr, C., Huffman, J. A., Cubison, M. J., Aiken, A. C., Docherty, K. S., Kimmel, J. R.,
13 Ulbrich, I. M., Hannigan, M., and Jimenez, J. L.: Characterization of primary organic aerosol
14 emissions from meat cooking, trash burning, and motor vehicles with high resolution aerosol
15 mass spectrometry and comparison with ambient and chamber observations, *Environ. Sci.*
16 *Technol.*, 43, 2443–2449, 2009.

17 Paatero, P.: Least squares formulation of robust non-negative factor analysis, *Chemom. Intell.*
18 *Lab. Syst.*, 37, 23–35, 1997.

19 Paatero, P.: The multilinear engine - A table-driven, least squares program for solving
20 multilinear problems, including the n-way parallel factor analysis model, *J. Comput. Graph.*
21 *Stat.*, 8, 854-888, 1999.

22 Paatero, P. and Tapper, U.: Positive matrix factorization - a nonnegative factor model with
23 optimal utilization of error-estimates of data values, *Environmetrics*, 5, 111-126, 1994.

24 Park, S.-S., Cho, S. Y., Jo, M. R., Gong, B. J., Park, J. S., and Lee, S. J.: Field evaluation of a
25 near-real time elemental monitor and identification of element sources observed at an air
26 monitoring supersite in Korea, *Atmos Pollut Res.*, 5, 119-128, doi:10.5094/APR.2014.015,
27 2014.

28 Pieber, S. M., El Haddad, I., Slowik, J. G., Canagaratna, M. R., Jayne, J. T., Platt, S. M.,
29 Bozzetti, C., Daellenbach, K. R., Fröhlich, R., Vlachou, A., Klein, F., Dommen, J., Miljevic,
30 B., Jimenez, J. L., Worsnop, D. R., Baltensperger, U., and Prévôt, A. S. H.: Inorganic salt

1 interference on CO₂⁺ in Aerodyne AMS and ACSM organic aerosol composition studies,
2 Environ. Sci. Technol., 50, 10494-10503, DOI: 10.1021/acs.est.6b01035, 2016.

3 Piot, C., Jaffrezo, J.-L., Cozic, J., Pissot, N., El Haddad, I., Marchand, N., and Besombes, J.-
4 L.: Quantification of levoglucosan and its isomers by High Performance Liquid
5 Chromatography – Electrospray Ionization tandem Mass Spectrometry and its applications to
6 atmospheric and soil samples, Atmos. Meas. Tech., 5, 141–148, doi:10.5194/amt-5-141-2012,
7 2012.

8 Poulain, L., Inuma, Y., Müller, K., Birmili, W., Weinhold, K., Brüggemann, E., Gnauk, T.,
9 Hausmann, A., Löschau, G., Wiedensohler, A., and Herrmann, H.: Diurnal variations of
10 ambient particulate wood burning emissions and their contribution to the concentration of
11 polycyclic aromatic hydrocarbons (PAHs) in Seiffen, Germany, Atmos. Chem. Phys., 11,
12 12697-12713, doi:10.5194/acp-11-12697-2011, 2011.

13 Rocke, D. M., and Lorenzato, S.: A two-component model for measurement error in
14 analytical chemistry, Technometrics, 37, 176-184, 1995.

15 Salameh, D., Detournay, A., Pey, J., Pérez, N., Liguori, F., Saraga, D., Bove, M. C., Brotto,
16 P., Cassola, F., Massabò, D., Latella, A., Pillon, S., Formenton, G., Patti, S., Armengaud, A.,
17 Piga, D., Jaffrezo, J.-L., Bartzis, J., Tolis, E., Prati, P., Querol, X., Wortham, H., Marchand,
18 N.: PM_{2.5} chemical composition in five European Mediterranean cities: a 1-year study,
19 Atmos. Res., 155, 102-117, 2015.

20 Salameh, D., Pey, J., Bozzetti, C., El Haddad, I., Detournay, A., Sylvestre, A., Canonaco, F.,
21 Armengaud, A., Piga, D., Robin, D., Prévôt, A. S. H., Jaffrezo, J.-L., Wortham, H., and
22 Marchand, N.: Sources of PM_{2.5} at an urban-industrial Mediterranean city, Marseille
23 (France): application of the ME-2 solver to inorganic and organic markers, Environ. Pollut.,
24 *submitted*.

25 Schauer, J. J., Kleeman, M. J., Cass, G. R., Simoneit, B. R. T.: Measurement of emissions
26 from air pollution sources. 3. C1-C29 organic compounds from fireplace combustion of
27 wood, Environ. Sci. Technol., 35, 1716–1728, 2001.

28 Schwarze, P. E., Ovreivik, J., Lag, M., Refsnes, M., Nafstad, P., Hetland, R. B., Dybing, E.
29 (2006). Particulate matter properties and health effects: consistency of epidemiological and
30 toxicological studies, Hum. Exp. Toxicol., 25, 559-579, 2006.

- 1 Seinfeld, J. H. and Pandis, S. N: Atmospheric chemistry and physics: from air pollution to
2 climate change, John Wiley, second Edn., New York, 2006.
- 3 Setyan, A., Zhang, Q., Merkel, M., Knighton, W. B., Sun, Y., Song, C., Shilling, J. E.,
4 Onasch, T. B., Herndon, S. C., Worsnop, D. R., Fast, J. D., Zaveri, R. A., Berg, L. K.,
5 Wiedensohler, A., Flowers, B. A., Dubey, M. K., and Subramanian R.: Characterization of
6 submicron particles influenced by mixed biogenic and anthropogenic emissions using high-
7 resolution aerosol mass spectrometry: results from CARES, *Atmos. Chem. Phys.*, 12, 8131-
8 8156, 2012.
- 9 Simoneit, B. R. T., Schauer, J. J., Nolte, C. G., Oros, D. R., Elias, V. O., Fraser, M. P., Rogge,
10 W. F., and Cass, G. R.: Levoglucosan, a tracer for cellulose in biomass burning and
11 atmospheric particles, *Atmos. Environ.*, 33, 173-182, 1998.
- 12 Simoneit, B. R. T., Sheng, G., Chen, X., Fu, J., Zhang, J. and Xu, Y.: Molecular marker study
13 of extractable organic matter in aerosols from urban areas of China, *Atmos. Environ. Part A.*
14 *Gen. Top.*, 25(10), 2111–2129, doi:10.1016/0960-1686(91)90088-O, 1991.
- 15 Slowik, J. G., Vlasenko, A., McGuire, M., Evans, G. J., and Abbatt, J. P. D.: Simultaneous
16 factor analysis of organic particle and gas mass spectra: AMS and PTR-MS measurements at
17 an urban site, *Atmos. Chem. Phys.*, 10:1969-1988, 2010.
- 18 Sullivan, A. P., Holden, A. S., Patterson, L. A., McMeeking, G. R., Kreidenweis, S. M.,
19 Malm, W. C., Hao, W. M., Wold, C. E., and Collett Jr., J. L.: A method for smoke marker
20 measurements and its potential application for determining the contribution of biomass
21 burning from wildfires and prescribed fires to ambient PM_{2.5} organic carbon, *J. Geophys.*
22 *Res.*, 113, D22302, doi:10.1029/2008JD010216, 2008.
- 23 Sun, Y., Zhang, Q., Zheng, M., Ding, X., Edgerton, E. S., and Wang, X.: Characterization and
24 source apportionment of water-soluble organic matter in atmospheric fine particles (PM_{2.5})
25 with high-resolution aerosol mass spectrometry and GC-MS, *Environ. Sci. Technol.*, 45,
26 4854–4861, 2011.
- 27 Ulbrich, I. M., Canagaratna, M. R., Zhang, Q., Worsnop, D. R., and Jimenez, J. L.:
28 Interpretation of organic components from positive matrix factorization of aerosol mass
29 spectrometric data, *Atmos. Chem. Phys.*, 9, 2891-2918, 2009.
- 30 Ulevicius, V., Byčenkienė, S., Bozzetti, C., Vlachou, A., Plauškaitė, K., Mordas, G., Dudoitis,
31 V., Abbaszade, G., Remeikis, V., Garbaras, A., Masalaite, A., Bles, J., Fröhlich, R.,

1 Dällenbach, K. R., Canonaco, F., Slowik, J. G., Dommen, J., Zimmermann, R., Schnelle-
2 Kreis, J., Salazar, G. A., Agrios, K., Szidat, S., El Haddad, I., and Prévôt, A. S. H.: Fossil and
3 non-fossil source contributions to atmospheric carbonaceous aerosols during extreme spring
4 grassland fires in Eastern Europe. *Atmos. Chem. Phys.*, 16, 5513-5529, 2016.

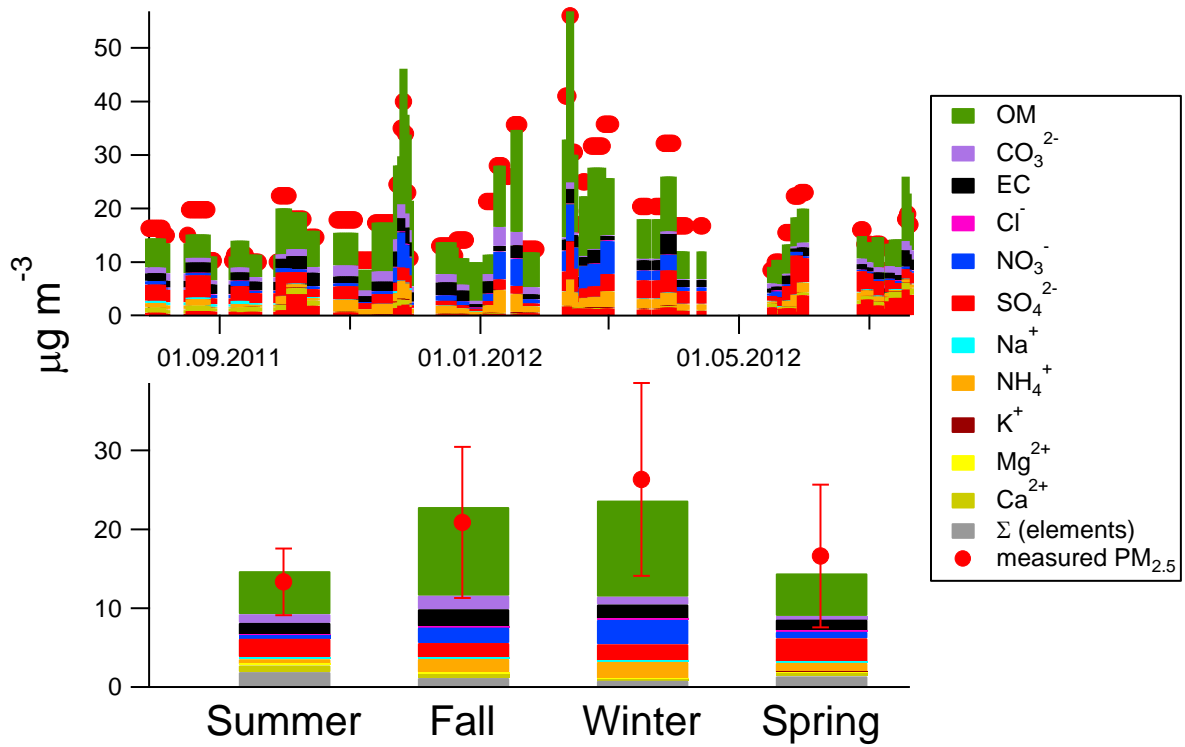
5 Weitkamp, E. A., Lipsky, E. M., Pancras, P. J., Ondov, J. M., Polidori, A., Turpin, B. J., and
6 Robinson, A. L.: Fine particle emission profile for a large coke production facility based on
7 highly time-resolved fence line measurements, *Atmos. Environ.*, 39, 6719–6733, 2005.

8 Zar, J. H., *Biostatistical analysis*, 4th ed., 929 pp., Prentice Hall, Englewood Cliffs, New
9 Jersey, 1999.

10 Zotter, P., Ciobanu, V. G., Zhang, Y. L., El-Haddad, I., Macchia, M., Daellenbach, K. R.,
11 Salazar, G. A., Huang, R.-J., Wacker, L., Hueglin, C., Piazzalunga, A., Fermo,
12 P., Schwikowski, M., Baltensperger, U., Szidat, S., and Prévôt, A. S. H.: Radiocarbon analysis
13 of elemental and organic carbon in Switzerland during winter-smog episodes from 2008 to
14 2012 – Part 1: Source apportionment and spatial variability, *Atmos. Chem. Phys.*, 14, 13551–
15 13570, doi:10.5194/acp-14-13551-2014, 2014.

16

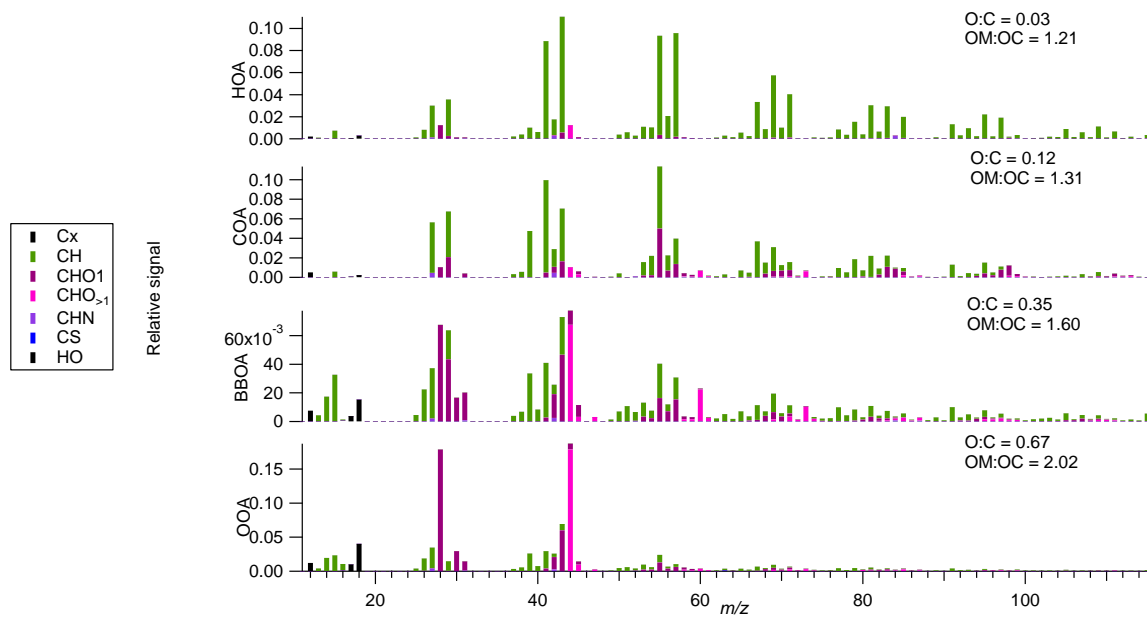
1



2

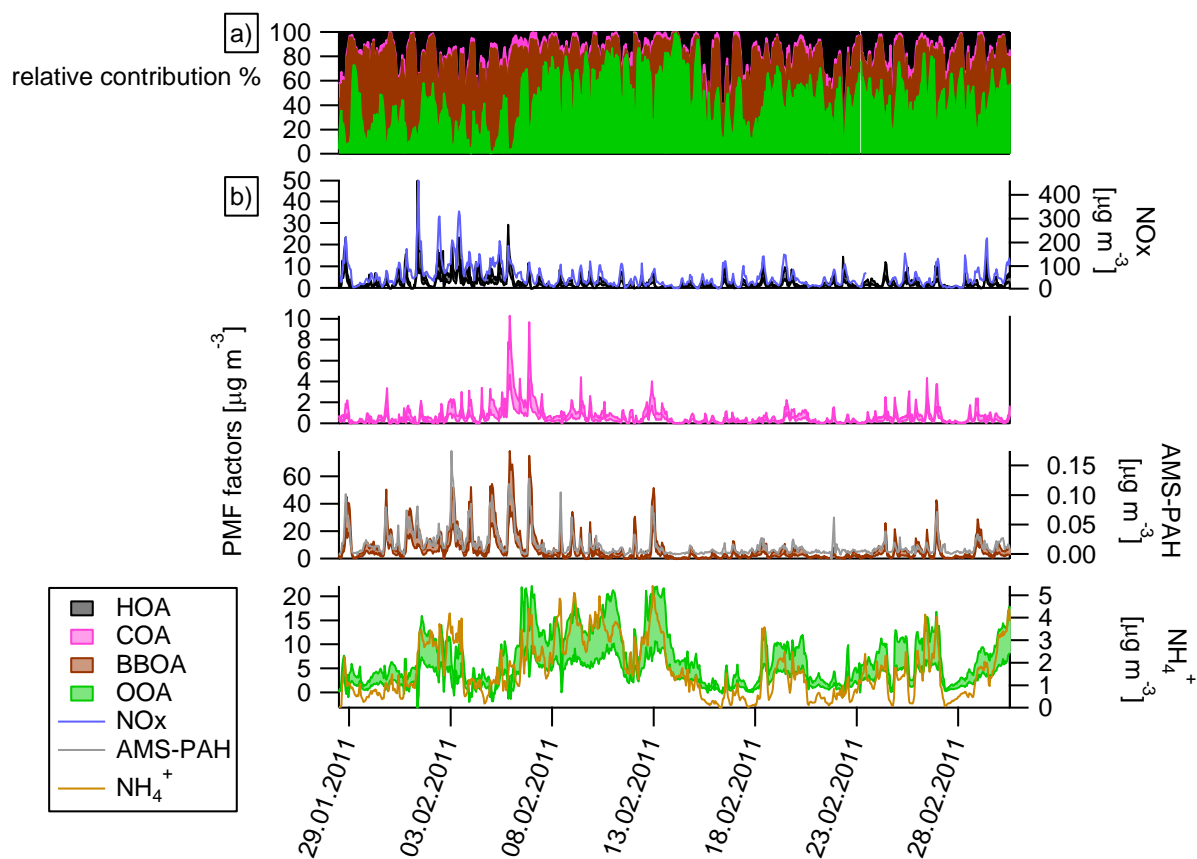
3 Figure 1. PM_{2.5} composition: stacked average seasonal concentrations. Measured PM_{2.5} error
4 bars represent the seasonal standard deviation. OM was estimated as the sum of the offline-
5 AMS source apportionment factors.

6



1

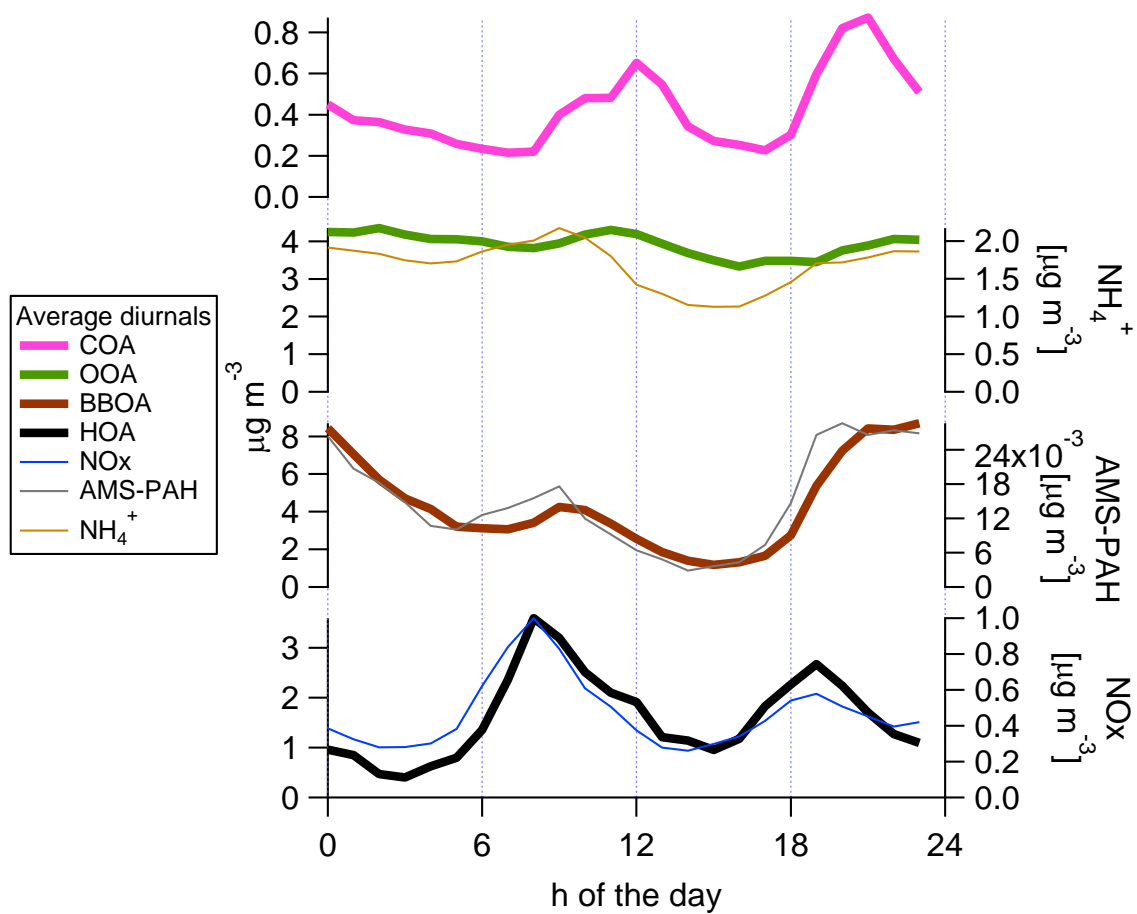
2 Figure 2. Online-AMS: average PMF factor mass spectra.



3

4 Figure 3. Online-AMS: a) PMF factors relative contributions. b) Time series of PMF factors
5 and corresponding tracers. Shaded areas denote the model uncertainties.

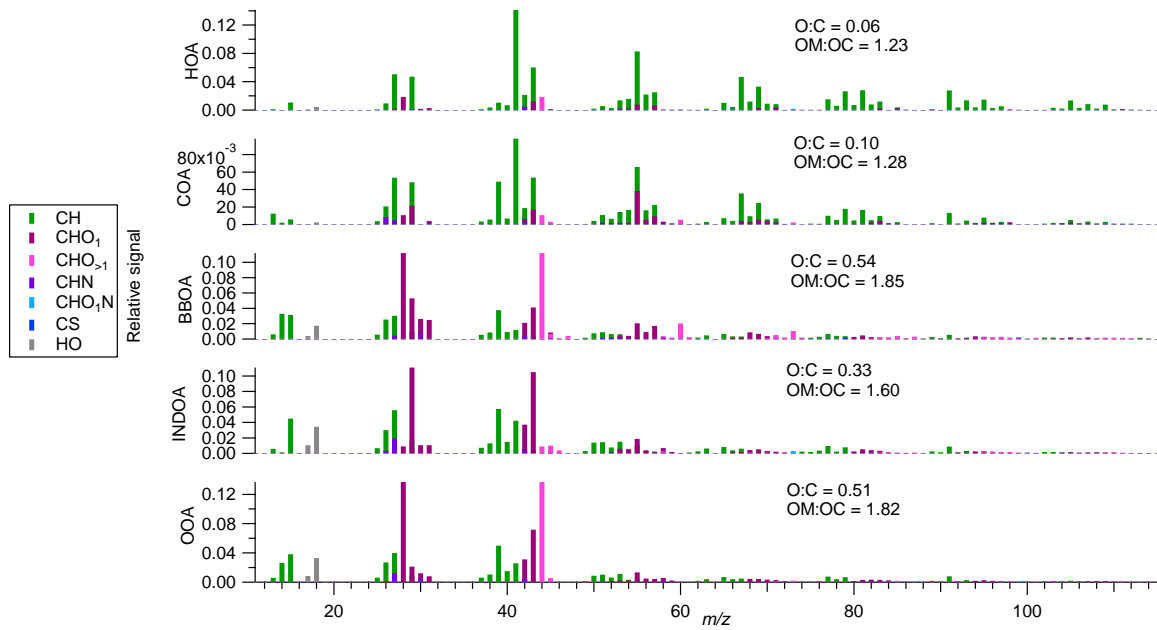
1



2

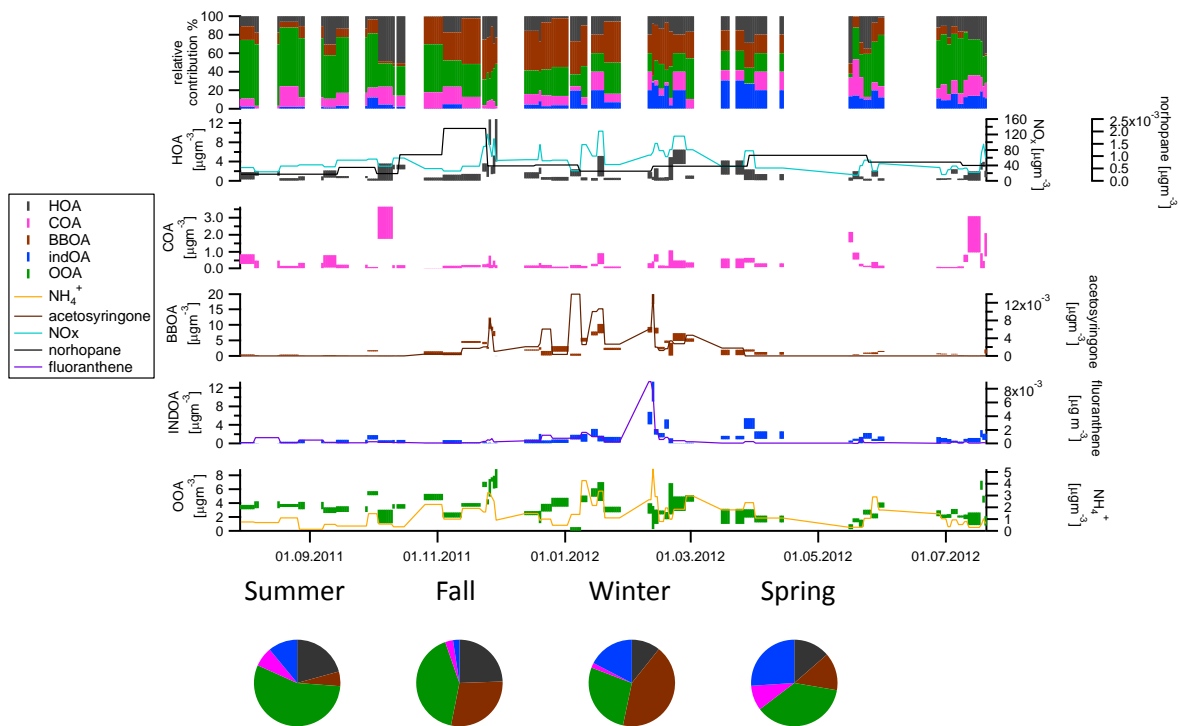
3 Figure 4. Online-AMS: average diurnal cycles of PMF factors and corresponding tracers.

4



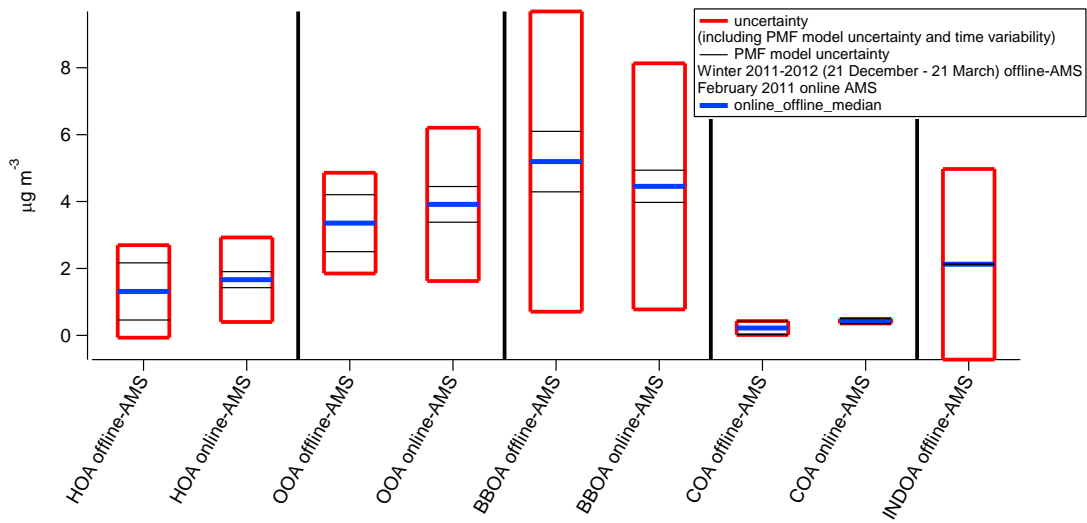
1
2 Figure 5. Offline-AMS: water soluble average mass spectra.

3
4
5



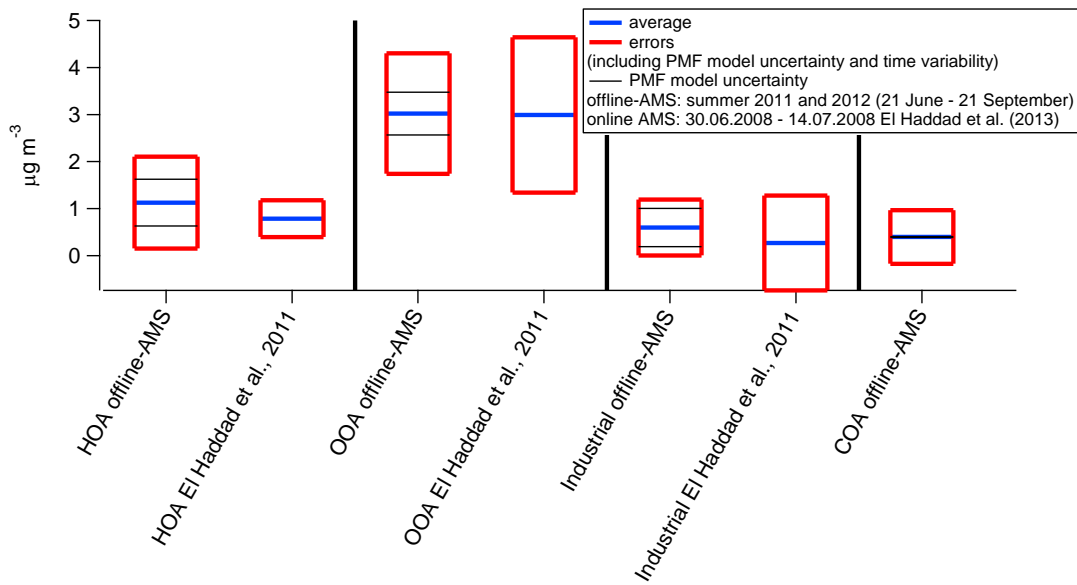
6
7 Figure 6. Offline-AMS: a) PMF factors relative contributions. b) Time series of PMF factors
8 and corresponding tracers. Bars denote the model uncertainties.

1



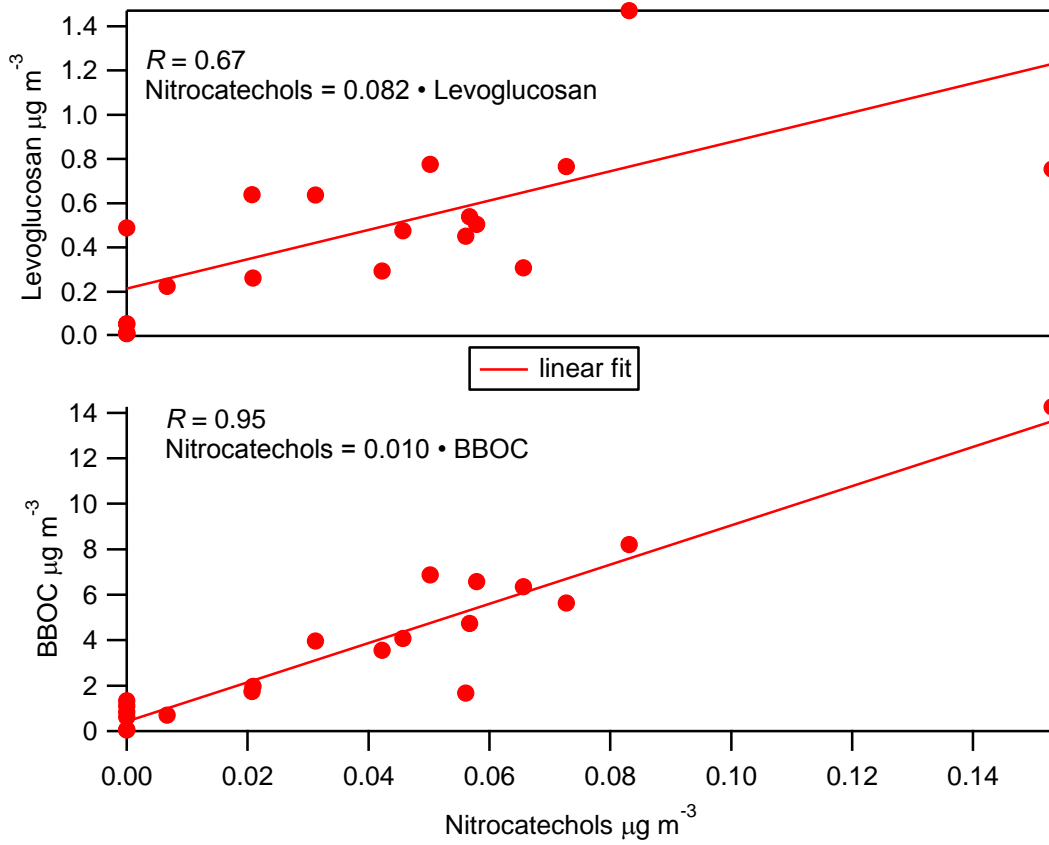
2

3 Figure 7. Online (PM_1) and offline-AMS ($PM_{2.5}$) comparison. Bars represent the error
4 including temporal variability and model uncertainty.

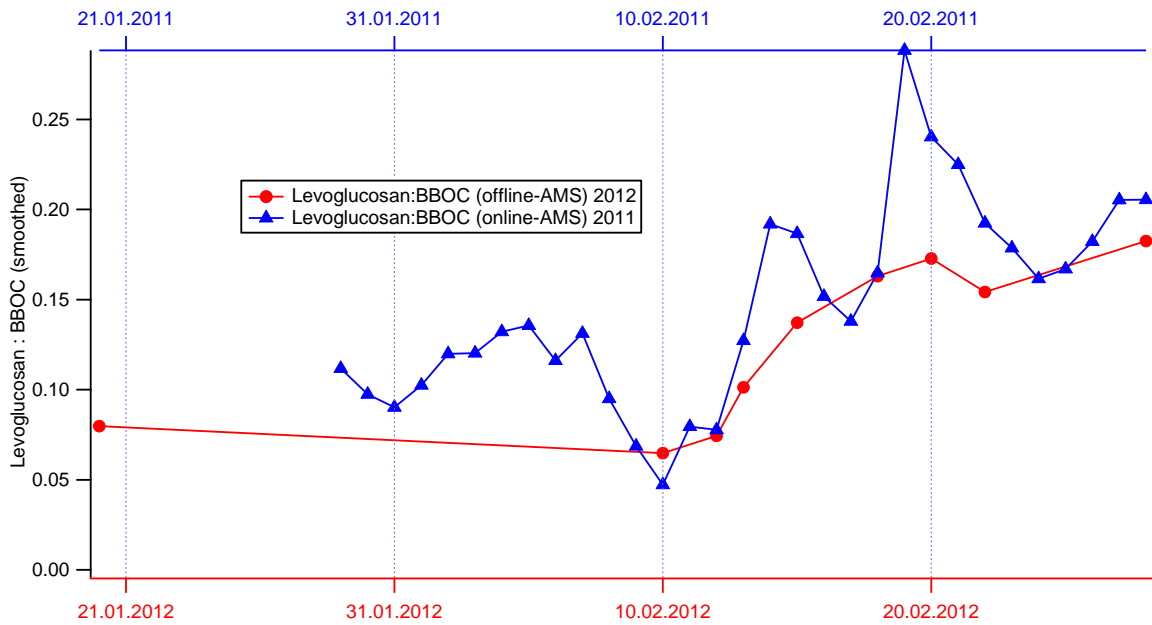


5

6 Figure 8. Online (PM_1 , El Haddad et al., 2013) and offline-AMS ($PM_{2.5}$) comparison. For
7 offline-AMS bars represent the error including temporal variability and model uncertainty.
8 For online-AMS bars represents only the temporal variability.

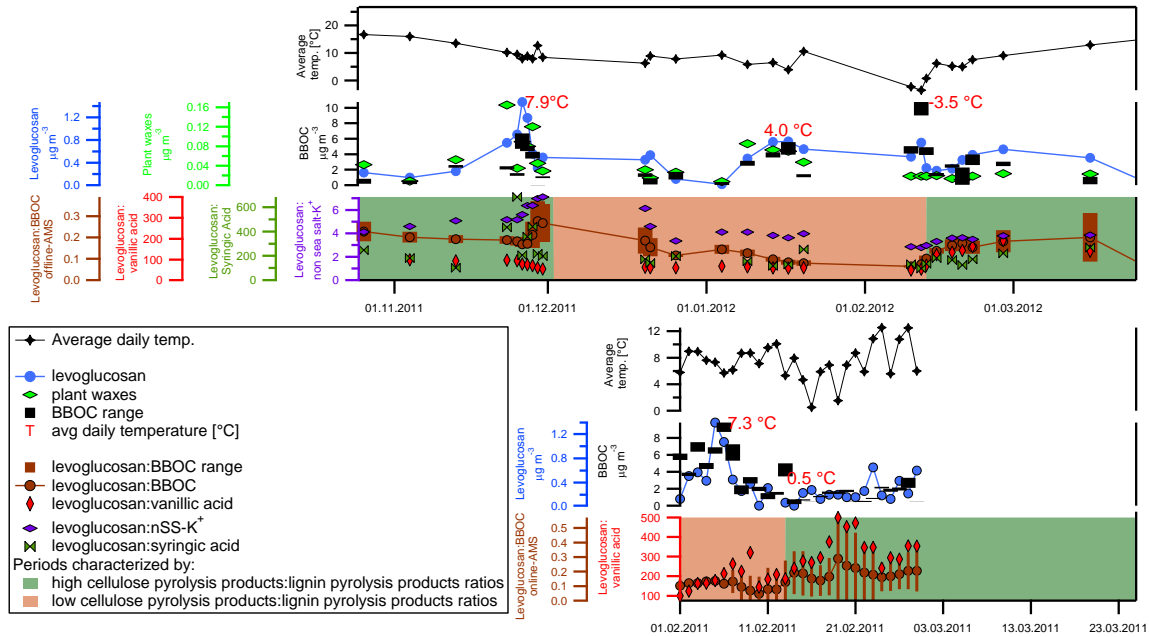


1
 2 Figure 9. Correlation between the sum of nitrocatechols (Table S1) with levoglucosan and
 3 BBOC.



5

1 Figure 10: Offline-AMS (February 2012) and online-AMS (February 2011) smoothed time-
 2 dependent levoglucosan:BBOC ratios. We note that the levoglucosan:BBOC comparison
 3 should not be considered on a day-to-day basis where the levoglucosan:BBOC ratio in the two
 4 different years can be coincidentally equal or different, but rather on a monthly time scale
 5 where, as discussed in the manuscript, we observed a statistically significant ($p=0.05$)
 6 evolution of the levoglucosan:BBOC ratio which is similarly captured by the two models.
 7
 8



9
 10 Figure 11: Online- and offline-AMS time-dependent levoglucosan:BBOC,
 11 levoglucosan:vanillic acid, levoglucosan:syringic acid, and levoglucosan: K^+ ratios. The plant
 12 waxes concentrations were determined from GC-MS measurements of alkanes with an odd
 13 number of carbons (Li et al., 2010). As discussed in the main text the spike observed in late
 14 autumn could be related to incomplete green waste combustion.
 15